ARTICLE

Integrating impedance cytometry with other microfluidic tools towards multifunctional single-cell analysis platforms

wReceived 00th January 20xx,
Accepted 00th January 20xx

DOI: 10.1039/x0xx00000x

Marta Righetto,[a] Cristian Brandi,[a] Riccardo Reale [a] and Federica Caselli *[a]

Microfluidic impedance cytometry (MIC) is a label-free technique that characterizes individual flowing particles/cells based on their interaction with a multifrequency electric field. The technique has been succesfully applied in different scenarios including life-science research, diagnostics, and environmental monitoring. The aim of this review is to illustrate the fascinating opportunities enabled by the integration of MIC with other microfluidic tools. Specifically, we identify five categories according to their synergistic advantage: (i) improving the multiparametric characterization capability, (ii) enabling on-chip sample preparation steps, (iii) stimulating the sample, (iv) sample carrying/confinement, and (v) impedance-activated sample sorting. We discuss examples from each category, highlighting integration challenges and promising perspectives for next-generation multifunctional systems.

1 Introduction

Single-cell analysis is essential to unveil the heterogeneity within a population of cells, which is often masked when analysing bulk cell samples. Alongside with traditional techniques such as single-cell sequencing and flow cytometry, biophysical cytometry[1] is emerging as a promising tool for label-free and non-destructive assays. Cell biophysical properties (e.g., morphological, electrical, and mechanical properties) reflect cell function and state in health and disease and are therefore natural biomarkers for diagnostics and treatment-response monitoring.

Microfluidics offers many opportunities to implement biophysical cytometry with high precision, sensitivity, and throughput.[2] This review deals with microfluidic impedance cytometry[3] (MIC), which is an electrical characterization technique based on the interaction between individual flowing cells, typically suspended in a conductive medium (~1 S/m), and an applied electric field. Depending on the frequency of the field, different cell properties are probed by MIC. From direct current (DC) to 1 MHz, the measured signal (i.e., an electric current) is mainly affected by cell size because the plasma membrane acts as a capacitive barrier. While DC impedance measurements need an even simpler instrument than alternating current (AC) measurements, they require tailored electrode materials/configurations (e.g., polyelectrolyte gel electrodes, PGEs) to mitigate issues arising from electrode polarization[4]. In the 2–10 MHz range, membrane polarization offers insights into membrane capacitance. Between 10–30 MHz, the membrane is minimally polarized, and measurements give information about cytoplasm permittivity and conductivity. At higher frequencies, the response is influenced by the properties of the nucleus. By applying a multifrequency electric field, MIC can simultaneously probe multiple cell properties. It is noticed that the specific frequency range values depend on cell size and on dielectric properties of cell and medium. In addition to the stimulation frequency, the design of the electrical sensing zone also plays a role in determining the type of information conveyed by the measured signals. With tailored electrode arrangements, cell motion properties (i.e., velocity and trajectory) as well as cell shape can be estimated. Overall, MIC offers a multiparametric single-cell characterization that has been employed in many applications, including e.g., cell viability assays,[5–7] cell activation/integrity studies,[8,9] antimicrobial susceptibility testing,[10–12] and stratification of cancer cells.[13] A comprehensive discussion on MIC principles and applications can be found e.g. in refs.[3,14–19].

MIC is a simple technique: it does not require labelling of the cell sample, the sensing element is just a microchannel with embedded electrodes, and the electronic acquisition system is suited for a portable implementation. Accordingly, the technique lends itself to being integrated with other microfluidic techniques, towards the development of multifunctional systems. This opportunity, which has been explored in the recent literature, is the focus of the present review. We identify five categories (Fig. 1), according to their synergistic advantage: (i) improving the multiparametric characterization capability, by coupling MIC with an additional sensing modality (Section 2); (ii) enabling on-chip sample preparation steps, to increase the accuracy of MIC measurements or to enrich selected populations prior to MIC analysis (Section 3); (iii) stimulating the sample, to elicit desired responses (Section 4); (iv) sample carrying/confinement into droplets or microcarriers, to provide tailored support or

[a] Department of Civil Engineering and Computer Science, University of Rome Tor Vergata, Rome, Italy. E-mail: caselli@ing.uniroma2.it.

microenvironment (Section 5); (v) impedance-activated sample sorting, to enable downstream analysis or reuse (Section 6). Such classification is not rigid and alternative points of view are possible. Furthermore, the same work may fit into more than one category. In such cases, the assignment is made according to the main aim/innovation of the work. The review is limited to systems involving MIC analysis of flowing (i.e., non-trapped) cells. As schematically illustrated in Fig. 1, the richness and variety of available microfluidic tools/approaches enable different possible combinations within each category. We discuss several examples, highlighting integration challenges and promising perspectives for next-generation single-cell analysis systems.

2 Integrating MIC with an additional sensing modality

In MIC, the raw data consist in the real part and imaginary part of electric current signals demodulated at different frequencies[3]. The passage of a particle in the sensing zone creates a variation of these signals, whose temporal shape depends on the chip layout and wiring scheme (most typically, in a differential measurement scheme, a bipolar Gaussian shape is found). Several features can be extracted from these signals, including (peak) amplitude and phase, opacity (i.e., the ratio of amplitudes at high versus low frequency), peak-to-peak times, and design-dependent features (e.g., prominence[20], tilt[21], anisotropy index[22]). The information content of such features depends on frequency and chip design. With multi-frequency stimulation and clever chip layouts, highly informative cell electrical fingerprints are built, which proved to be effective in many cell analysis tasks, such as cell subpopulation analysis and cell treatment-response monitoring.

During the development of MIC, microfluidic devices integrating MIC sensing with another sensing modality have been developed. In these works, the additional sensing feature was included to validate the impedance measurement and to obtain insight into the meaning of the electrical features[23–28]. On the other hand, the opportunities provided by multimodal approaches over single sensing have emerged. Multimodal approaches combine two (or more) distinct sensing methods, each of which analyses different types of cell/particle properties, thus allowing an enhancement of the accuracy of cell/particle identification compared to using either technique alone. Exploring this direction, MIC sensing has been integrated with optical flow cytometry (Section 2.1), imaging flow cytometry (Section 2.2), and microwave sensing (Section 2.3). An overview of these systems is provided in Table 1.

2.1 MIC and optical flow cytometry

Optical flow cytometry is an essential technology in contemporary biomedical research and clinical practice, enabling high-throughput and high-resolution analysis of cells and particles based on light scattering and fluorescence. In recent years, significant research efforts have been directed toward the development of microfluidic optical flow cytometers, driven by the need for more compact, cost-effective, simplified, and autonomous alternatives to conventional flow cytometers[4].

Aiming at developing highly informative systems, a few microfluidic devices integrating both optical and impedance sensing have been reported. Holmes et al. [29] (Fig. 2A) developed a microfabricated flow cytometer designed to count and analyse micro-sized polymer beads used as solid supports for fluorescence immunoassays. The system used laser excitation and commercially available data acquisition cards for signal collection. Impedance measurements of the particles were used to accurately determine their size and to trigger fluorescence data collection. Specifically, the device quantitatively assessed antibody binding to surface-immobilized antigens by measuring fluorescence at 532 nm and 633 nm wavelengths. A portable PCB-based system to simultaneously detect impedance and fluorescence was introduced by Joo et al. [4] (Fig. 2B). DC impedance detection captured data about the presence and size of microparticles and cells via PGEs, while fluorescence was measured using a LED for excitation and a solid-state photomultiplier (SSPM) for detection, thus limiting the size, cost, and power consumption of the system.

Further developments towards a multiparametric characterization have been introduced by Spencer et al. [30] (Fig. 2C) who presented a compact, sheath-less micro-cytometer capable of measuring four key parameters: fluorescence, large angle side scatter, and electrical impedance at two frequencies (for electrical volume and opacity). This device was tested using haemolysed human blood, where it successfully performed a four-part differential leukocyte assay (i.e., neutrophils, monocytes, CD4+ lymphocytes, CD4- lymphocytes). Differentiation of blood cells was also reported by Simon et al. [31]. Their system demonstrated label-free discrimination of lymphocytes, monocytes, neutrophils, and eosinophils in haemolysed blood samples by integrating impedance at a single frequency with light side scatter (SSC) data.

In the study by Honrado et al. [32], MIC was used to analyse the dielectric properties of *Plasmodium falciparum*-infected red blood cells (i-RBCs) at various stages of the intraerythrocytic life cycle. The parasites within the host cells were identified using the green fluorescent protein (GFP) emission, allowing for clear differentiation of infected cells. The simultaneous measurement of fluorescence and impedance allowed direct correlation of electrical and fluorescent properties at the single-cell level. This research shed light on the dynamic changes in the host cell membrane and the parasite as the infection progresses.

Recently, Liang et al. [33] introduced a microfluidic flow cytometry platform that can simultaneously quantify key intrinsic structural and electrical parameters of single cells, including cell diameter (D_c), nuclear diameter (D_n), cytoplasmic conductivity (σ_{cy}), and specific membrane capacitance (C_{sm}). This platform incorporates a double T-type constriction channel and a fluorescence detection region. As cells pass through the constriction, D_c, σ_{cy}, and C_{sm} are derived from impedance signals, while D_n is determined using fluorescence signals. The

platform was validated by accurately characterizing these parameters in three established carcinoma cell lines. Additionally, when applied to leukemia and oral tumor samples, the simultaneous assessment of D_c, D_n, σ_{cy}, and C_{sm} improved cell-type classification success rates, outperforming methods that rely on individual biophysical markers alone.

2.2 MIC and imaging flow cytometry

While optical flow cytometry yields cell integrated data using single pixel detectors (e.g. photomultiplier tubes), in imaging flow cytometry spatially resolved images of single flowing cells are captured using high-speed cameras with a 2D pixel array, enabling the analysis of morphological cell features [34]. The combination of imaging flow cytometry and MIC has been recently reported in a few works. For instance, D'Orazio et al. [35] (Fig. 2D) introduced a multimodal approach that integrates electrical sensing and optical imaging to classify pollen grains. This method processes electrical features and optical features using two independent support vector machines (SVM) classifiers. Their outputs are combined to establish the final classification result. The approach outperforms methods based solely on electrical or optical features, as shown in a case study involving eight pollen classes. A similar approach was implemented by Kokabi et al. [36], who exploited the combination of electrical and optical properties in a multimodal method for the classification of paramagnetic beads of different sizes and breast cancer cells.

Chen's group [37,38] introduced a microflow cytometer designed for high-throughput characterization of electrical and structural properties of single cells. The cells are confined within a microchannel constriction, allowing high-quality image capture of the cell [38] or the nucleus labeled with fluorescence [37] without loss of focus. Electrical and structural features are extracted from impedance profiles and optical images via either traditional or deep learning approaches. These features are then combined for cell-type classification via SVM. In ref. [37], by extracting six critical biostructural and bioelectrical features, such as cell size, nuclear shape, and cytoplasmic conductivity, from thousands of individual cells, an accuracy of 88.3% was achieved in distinguishing between A549, Jurkat, and K562 cells using a feedforward neural network. Additionally, deep learning models, i.e., VGG16 convolutional neural network (CNN) and Long Short-Term Memory (LSTM) recurrent neural network (RNN), were applied to analyze fluorescent images and impedance data, resulting in nearly 100% accuracy in cell type identification. In ref. [38] (Fig. 2E), two leukemia cell lines (HL60 and Jurkat) were analyzed, achieving classification accuracy of 99.3% based on electrical features extracted using LSTM networks of the RNN, 96.7% based on structural features from ResNet18 of the CNN, and 100% when combining features using SVM. Furthermore, a systematic study to compare various bimodal fusion strategies in processing single-cell impedance and images was recently reported in ref. [39].

2.3 MIC and microwave sensing

Microwave resonant sensors have emerged as a promising electronic method for analyzing non-biological microparticles [40,41]. These sensors operate in the microwave frequency range (GHz), thus avoiding Debye shielding effects, and can measure the capacitance of microparticles. Such capacitance is a function of the size of the particle and of its Clausius–Mossotti (CM) factor, which in turn depends on the complex permittivity of the particle and the medium. Tefek et al. [40] (Fig. 2F) designed a sensing platform integrating impedance cytometry at 500 kHz with microwave resonant sensing at 5 GHz. The microwave signal, affected by both permittivity and size effects, can be normalized using the size data from impedance cytometry, resulting in a parameter dependent on permittivity alone. This method enables the distinction between microparticles (polystyrene and soda lime glass of similar sizes) based on permittivity differences, with an accuracy exceeding 94%, despite their close size and electrical properties. Additionally, the same technique can differentiate between healthy cells and fixed cells of identical geometric size.

2.4 Section summary

The integration of MIC with other sensing modalities is driven by the need to increase the measurement's information content, which can be pivotal to address complex biological targets. MIC's ability to probe dielectric properties of cell elements (e.g. cell membrane capacitance and cytoplasmic conductivity) is well complemented with methods characterizing cell morphology (e.g., overall shape, nuclear boundary) and cell molecular content (via fluorescence analysis). These multiparametric measurements are more informative than their individual counterparts and often lead to significant improvements in diagnostic performance (e.g. accuracy, sensitivity). The integration of different sensing modalities is further boosted by recent developments in artificial intelligence approaches, which allow to simultaneously analyse measurement data-streams deriving from different techniques. From a setup point of view, MIC is readily integrated with additional sensing modalities employing electric fields (electrodes for both modalities can be manufactured in the same fabrication step) or light (MIC chips usually have a clear glass substrate providing free optical access to the sample). As a perspective, MIC promises advantage for both the integration with other label-free methods, when keeping the benefit of non-invasiveness is critical, as well as with label-based methods, when higher specificity is required.

3 Integrating MIC with on-chip sample preparation

On-chip approaches for sample preparation prior to impedance measurements belong to two main groups: sample focusing to improve measurement accuracy (Section 3.1) and selection/enrichment of target subpopulations in heterogenous samples (Section 3.2).

3.1 Sample focusing towards improved accuracy

Particle focusing methods are techniques used to align and concentrate particles into a narrow stream within a fluid flow. These methods are crucial for applications like cell counting, characterization, and sorting, and are widely used in microfluidic devices. Focusing particles ensures that they pass through detection or sorting regions one at a time and in a consistent manner, which enhances the accuracy of measurements, reduces the likelihood of coincident events, and prevent channel blockage due to particles adhesion to the microchannel walls. Particle focusing approaches belong to two main categories: sheath flow focusing and sheathless focusing. The former methods use one or more sheath fluids to pinch the particle suspension, thereby focusing the particles into a tight stream. Sheathless focusing can be divided into active focusing, where external forces such as electric, magnetic, or acoustic fields are used to focus particles, and passive focusing, which uses the inherent fluid dynamics and channel geometry to achieve particle focusing (e.g., inertial and elasto-inertial focusing). A comparative analysis of the different techniques can be found e.g. in Refs. [42–44].

In the specific context of MIC, particle focusing methods are useful to improve measurement accuracy. In fact, to record signals with high signal-to-noise ratio (SNR), the volume of the sensing zone should be commensurate to the volume of the particle to be analysed (the most critical dimension being channel height for facing electrode designs and electrode distance for coplanar electrode designs). This poses challenges in applications dealing with small (submicron) particles, since channels with small cross-section are difficult to fabricate and prone to clogging, or for mechanically sensitive bioparticles (e.g., platelets) that can be altered/activated by large shear forces. To virtually reduce the volume of the sensing zone while maintaining a relatively large channel cross-section, dielectric focusing has been proposed: cells are suspended in a conductive core stream whose diameter is comparable to cellular dimensions, while the core is sheathed by a dielectric, non-conductive fluid. Larsen et al.[45] first suggested the use of a non-aqueous phase to confine the sample in 1D, however the surface tension at the interface between the two phases caused flow instabilities and therefore noisy measurements. Bernabini et al.[46] solved this problem by adding small amount of surfactant to the non-aqueous phase and demonstrated the discriminate between 1 µm and 2 µm diameter beads and between *Escherichia coli* (*E. coli*) and 2 µm beads. Choi et al. [47] developed a submicron-sized bacterial detection system: by introducing a movable virtual wall made of a non-conducting oil solution, they could precisely adjust the effective channel width by regulating the flow rate of the wall solution. Lateral dielectric focusing combined with vertical dielectrophoretic (DEP) focusing was used by Evander et al. [48] (Fig. 3A) for platelet analysis. Their system demonstrated increased SNR while minimizing shear forces and therefore platelet activation caused by the microfluidic chip. Impedance cytometers with 1D or 2D dielectric focusing using an aqueous sheath fluid (e.g., distilled water) were also developed[49–51], with the first example being reported by Nieuwenhuis et al.[52]. However, using an aqueous phase for both the sheath and the sample liquids requires to account for ion diffusion from the sample liquid into the sheath liquid. A systematic study on how to choose the sheath liquid to enhance the accuracy was reported by Zhu et al. [53], who suggested the use of a viscous non-conductive polyethylene glycol (PEG) solution.

Besides the SNR, another aspect to account in MIC is the positional dependence[54] of the measured signals, i.e., identical particles flowing along different trajectories provide different signals due to the non-uniformity of the electric field (which is more pronounced in coplanar electrode designs). Positional dependence is unwanted when performing cell subpopulations analysis, since it introduces a blurring on the measured cell properties. To overcome this issue, several on-chip particle focusing mechanisms have been proposed, including hydrodynamic, inertial, acoustophoretic, and DEP focusing. For instance, Zhou et al.[55] developed a hydrodynamic focusing mechanism to adaptively concentrate the sample laterally and vertically at the bottom of the microchannel, reducing the variance of particle translocation height and increasing the overall SNR. Tang et al. [56,57] (Fig. 3B) used an asymmetric serpentine structure and elasto-inertial focusing to achieve consistent cross-sectional position of tumor cells, therefore minimizing the fluctuation of impedance responses due to position blurring. Specifically, the asymmetric serpentine structure allows to focus cells along the channel width, while elasto-inertial focusing ensures a single focusing position along channel height. Two-dimensional particle focusing was also demonstrated by Grenvall et al. [58] (Fig. 3C), using acoustic forces: the fundamental vertical as well as the horizontal resonance mode of the channel cross section were simultaneously excited using two piezoceramic transducers actuated at 2 and 5.3 MHz respectively. A comprehensive review of the strategies developed to reduce position influence in impedance-based assays is reported in Ref.[16].

In the case of non-spherical particles/cells, such as in applications dealing with particle shape/deformability, the measured signals also depend on particle orientation. Accordingly, particle orientation mechanisms have been developed. Shaker et al. [22] used DEP focusing to align rod-shaped particles and buddying yeasts in the direction orthogonal to flow, before MIC measurements. The latter were performed along two orthogonal directions, to extract an electrical index of particle shape anisotropy. Xie et al. [59] designed an impedance cytometer with three constricted structures to focus and orient particles at the sensing zone. Specifically, the constricted structures induced velocity gradients and pressure steps that aligned elongated particles along the streamline.

3.2 Selection/enrichment of populations

Many applications in single-cell analysis require the selection/ enrichment of specific, possibly rare, cell populations. To this aim, several microfluidic cell separation techniques have been developed. Their comparative analysis can be found e.g. in refs. [60]. An overview of MIC systems with integrated

selection/enrichment of specific cell types, described in the following, is provided in Table 2.

Among possible application scenarios, the isolation, analysis, and quantification of circulating tumor cells (CTCs) from blood is crucial for cancer diagnosis, prognosis, and treatment monitoring. Han et al.[61] (Fig.3D) introduced a microfluidic device designed for the enrichment and electrical discrimination of CTCs labelled with immunomagnetic nanobeads (MNBs) and graphene nanoplates (GNPs). In the first step, the CTC-enrichment module, MNBs and lateral magnetophoresis are used to isolates rare CTCs from millions of background blood cells. In the second step, impedance cytometry identifies the CTCs from the residual blood cells based on signal amplitude (which correlates with cell size) and signal phase (which reflects the electrical properties of GNP-modified CTCs). A label-free CTC enrichment approach was developed by Raillon et al. [62] integrating MIC with a vortex plastic chip that isolates cancer cells using inertial microfluidics and microscale vortices. Since CTCs are larger than red blood cells (RBCs) and most white blood cells (WBCs), they are stably captured in the microvortices, while blood cells flow through the main channels. The vortex chip successfully enriched the cancer cells, which were then counted and distinguished from smaller blood cells by the impedance chip based on size.

Other application-relevant cells are circulating leukocytes, an essential component of the immune system. Rapid analysis of their natural state and functions can provide valuable insights into their roles in disease processes, helping to discover new prognostic biomarkers for health and disease [63]. The inertial-impedance cytometry system developed by Hou's group [63,64] incorporates a Dean Flow Fractionation (DFF) sorting mechanism, an asymmetrical serpentine focuser, and an impedance sensor for continuous, rapid, label-free sorting and single-cell electrical profiling of leukocytes. In the DFF sorter, particles of different sizes experience distinct lateral movements due to the combined effects of inertial and Dean flows in curved channels. This process directs larger cells to stabilize near the top wall, while smaller particles and the sample's aqueous phase flow toward the bottom wall. In ref. [63], the multi-stage platform isolates neutrophils and monocytes directly from diluted or lysed blood, while in ref. [64] (Fig. 3E), it isolates neutrophils directly from urine samples. After isolation, impedance phenotyping is performed. This "sample-in-answer-out" platform has potential to be further developed into a point-of-care testing technology.

Han et al. [65] introduced an integrated microfluidic platform that enables comprehensive blood analysis through MIC. The system features a specially designed microfluidic network for lysing RBCs. Utilizing a multistep lysis approach, the system efficiently prepares clinical blood samples for subsequent cell identification and counting via MIC. Bashir's group [66,67] (Fig. 3F) developed a microfluidic biochip that enables direct counting of specific lymphocyte types, such as CD4+ and CD8+ T cells, from whole blood, which is critical for research and diagnostic uses like HIV/AIDS monitoring. These biochips function without external sample preparation, employing differential electrical counting across five integrated modules that sequentially lyse RBCs, protect leukocytes, count cells electrically, capture target cells via antibody-coated microposts, and re-count the remainder. The microchip uses shear-stress immunocapture to deplete target cells efficiently, optimizing T cell isolation by lysing RBCs to focus on WBCs. Antibodies in the microfluidic channels capture CD4+ or CD8+ T cells specifically, and the system can be adapted to count other cell types by modifying the antibodies in the capture chamber.

Torres Castro et al. [68] (Fig. 3G) developed an integrated microfluidic platform that combines deterministic lateral displacement (DLD) for cell separation with downstream impedance cytometry to effectively enrich activated macrophages from mixed cell populations, avoiding sample loss and dilution common in off-chip analyses. The system processes samples with both activated and unactivated macrophages, selectively enriching activated macrophages based on increased cell size and impedance characteristics.

The combination of MIC and automatic sampling was also presented, for accurate bioaerosol detection. Specifically, Lee at al. [69] presented a cyclone-cytometer integrated air monitoring system (CCAM), developed by combining a wet-cyclone air sampler with a DC impedance microfluidic cytometer. The wet-cyclone sampler first collects airborne particles, concentrating them into a 10 mL aqueous solution within 5 minutes. This solution, containing bioaerosols, is then directly transferred to the microfluidic cytometer, where it undergoes size-based particle analysis without any need for pretreatment. Tested with microbeads, mineral dust, and both live and dead *E. coli*, CCAM demonstrates high accuracy in distinguishing particles from 0.96 to 2.95 μm.

3.3 Section summary

Most on-chip sample preparation features that have been integrated with MIC belong to particle focusing approaches. Apart from dielectric focusing, which is tailored to MIC, those approaches are also widely used in optical or image flow cytometry, which share with MIC the issues of position-induced measurement blurring and coinciding events. On the other hand, MIC systems that do not need particle focusing are also available. The latter are based either on designs that maximize the uniformity of the electric fields or on clever signal processing[16]. A few MIC systems with integrated selection/enrichment of specific cell types (mainly rare cells or blood cells subpopulations) were also reported. Since the specificity of MIC is limited compared to characterization techniques relying on cell surface markers, reducing the complexity of heterogeneous samples prior to MIC analysis can be highly relevant in some applications.

4 Integrating MIC with on-chip sample stimulation

Several MIC systems integrating some form of on-chip sample stimulation have been developed, including mechanical (Section 4.1), electrical (Section 4.2), or physicochemical

(Section 4.3) stimulation. An overview of these systems is provided in Table 3.

4.1 Mechanical stimulation

The mechanical properties of cells have emerged as valuable label-free biomarkers for studying and characterizing cells[70]. Deformability, the cell's ability to change shape in response to external forces[71], is linked to various molecular changes and has been established as a key mechanical biomarker for diagnosing diseases such as cancer, malaria, diabetes, and sickle cell anemia. For instance, cancer cells are generally more deformable than normal cells, facilitating tissue invasion[72]. Furthermore, deformability of RBCs is crucial for maintaining blood flow in the microvasculature, with decreased deformability contributing to increased flow resistance in diseases like diabetes and malaria[73]. Measuring cell mechanics at the single-cell level is also essential for applications in immune system analysis and drug development. Microfluidic technologies offer new high-throughput methods for assessing cell deformability with improved accuracy and sensitivity[74]. Within this framework, MIC-based deformability cytometers have been developed by coupling electrical sensing with on-chip mechanical stimulation, either using microconstriction or contactless approaches based on hydrodynamic deformation.

Microconstriction-based approaches. Zhou et al. [70] developed a microfluidic device that assesses cell deformability based on the passage time of the cell through a microchannel constriction. The passage time is measured using electrical impedance signals. Specifically, by using four electrode pairs, the total passage time is divided into entry time (related to deformability) and transit time (influenced by friction between the cell and the channel walls). Furthermore, cell impedance magnitude is also measured, to improve cell characterization. Yang et al. [75] further developed this approach by introducing a differential multiconstriction device that allows measuring a cell relaxation index, besides deformability and electrical impedance. In fact, proper cell relaxation behavior is important in cell migration and in maintaining structural integrity. Both studies highlight that combining mechanical and electrical properties enhances cell population differentiation.

Ghassemi et al. [76] used a simple design based on a constriction channel with integrated electrodes to detect and count CTCs in blood samples. The sensor measures impedance, both in terms of magnitude and phase, at various frequencies as the cells pass through the constriction. Due to the deformable nature of cancer cells as they move through the channel, compared to the consistent shape of blood cells, unique impedance patterns were produced, which allowed for the accurate identification and counting of CTCs. Han et al. [77] introduced a microfluidic platform capable of assessing both the mechanical and electrical characteristics of individual plant cells. In their device, cells were aspirated through a constriction channel, where the impedance sensor measured the time taken for cells to pass, reflecting cell deformability. This technique distinguished cells based on their stiffness, with plant cells that have a primary cell wall (PCW) showing lower deformability and electrical conductivity.

Recently, Feng et al. [78] (Fig. 4A) introduced a camera-free intrinsic mechanical cytometry (CFIMC) technique for real-time measurement of two key mechanical properties of single cells: Young's modulus (E) and fluidity (β). The power-law rheological model is used to resolve E and β from impedance signatures. With a throughput of 500 cells per minute, this method effectively distinguishes mechanical differences between cancerous and normal cells (MCF-10A, MCF-7, and MDA-MB-231), between live and fixed cells, and in response to pharmacological treatments affecting the cytoskeleton. In a subsequent work[79] , a multimodal system was proposed that uses time-division multiplexing to simultaneously capture both electrical and mechanical deformability data from the impedance signal. Consequently, multiple biophysical parameters, including radius (r), cytoplasm conductivity (σ_i), specific membrane capacitance (C_{sm}), E, and β, can be measured in a single pass. The enhanced system demonstrated its capability by achieving a 93.4% classification accuracy in differentiating three types of cancer cells, surpassing the accuracy of systems relying solely on either electrical or mechanical measurements.

Contactless approaches. Contactless approaches have also been explored to overcome the limitations of constriction-based systems, which are effective only for specific cell size ranges and can be prone to clogging. To induce contactless cell deformation, hydrodynamic techniques have been employed. Reale et al. (Fig. 4B) [71] introduced a microfluidic system that integrates (i) a hyperbolic microchannel to induce RBCs deformation through viscoelastic extensional flow and (ii) an electrical sensing zone with four coplanar electrodes arranged in a cross, to probe cell impedance along two orthogonal directions. The system deforms RBCs and measures cell shape changes using an electrical anisotropy index (i.e., the ratio of the impedance signals along the orthogonal directions), with a throughput of 300 cells per second. To mitigate position-induced blurring, a gating on cell velocity is implemented. Tests on healthy and chemically stiffened RBCs demonstrated that the anisotropy index reliably indicates RBC deformability. A subsequent system using viscoelastic extensional flow, electrical sensing, and machine learning was recently presented to discriminate pancreatic cancer cells and cancer associated fibroblasts based on their deformability and electrophysiology [80]. In this system, utilization of viscoelastic flows enables elasto-inertial particle focusing across the microchannel depth, thereby minimizing positional dependence. Hou's group [81,82] developed a deformability cytometer integrating viscoelastic-inertial focusing, hydrodynamic cell pinching via sheath fluids, and impedance-based techniques for cell analysis. They employed an electrical deformability index, derived from the differential impedance patterns of both native and deformed cells, to mechanically phenotype HL-60 cells and human neutrophils [81] (Fig. 4C) and to identify residual induced pluripotent stem cells (iPSCs) at low abundance among spinal cord progenitor cells (SCPCs) [82]. Furthermore, viscoelastic shear flow was used by Morgan's group [83] to induce cell deformation.

As in ref. [71], the latter was quantified from the ratio of two impedance signals along orthogonal directions, by using arrays microelectrodes. Electrical deformability was validated by comparison with optical deformability [28], measured using a low-cost CMOS camera illuminated with a high-power LED triggered by the MIC signal.

4.2 Electrical stimulation

Electrical stimulation can be used to temporarily open pores in the cell membrane, thus allowing for the delivery of therapeutic and diagnostic substances, such as nucleic acids, proteins, and nanoparticles[84]. Electroporation is widely used in biomedical research and clinical applications and is preferred over viral methods for cell transfection due to its safety, efficiency, and wide applicability. However, optimizing electroporation protocols for different cell types and payloads is crucial to ensure effective delivery while maintaining cell viability. Advanced microfluidic platforms now enable high-throughput, controlled single-cell electroporation with real-time detection of membrane permeability.

In a pioneering work, Burgel et al. [85] (Fig. 4D) developed a chip-based platform for manipulating, electroporating, and analyzing single mammalian cells in suspension without labeling. This system allows flow reversal, enabling multiple MIC measurements of the same cell in seconds, supporting either analysis over time or averaging for greater precision. The platform efficiently electroporates cells using an 8 V, 50 kHz electrical stimulus, while MIC monitors and quantifies the electroporation process and its effects. It enables precise measurement of cellular changes and dielectric properties, offering detailed insights and control.

A few works integrated electroporation with constriction-based microchannels to enhance electroporation efficiency. Zheng et al. [84] developed a microdevice capable of detecting, electroporating, and monitoring individual cells for changes in permeability and molecular delivery within a continuous-flow system. Their design offers three key advantages: (i) strong current signals for single-cell detection, (ii) high SNR for impedance changes during permeabilization, and (iii) electroporation pulse amplification through geometric constriction, reducing voltage requirements and minimizing adverse effects like heating and electrolysis. A viability of 86% or higher was found for cells that underwent electroporation treatment at 0.7 or 0.87 kV/cm, indicating complete resealing of the cell membrane within 20 minutes post-permeabilization. A similar system was presented by Ye et al. [86] (Fig. 4E): as individual cells pass through a narrow microchannel, a concentrated electric field is applied to their membranes, achieving an electroporation efficiency of up to 96.6%. Additionally, simultaneous impedance measurements enable precise detection of the electroporation event and provide insights into the extent of permeabilization for each cell. A key advantage of all these systems is their ability to facilitate analysis both before and after electroporation without the need for cell immobilization.

4.3 Physicochemical stimulation

MIC has also been used to monitor cellular response to different types of physicochemical stimulations. For instance, Du's group [87] developed an electrical impedance-based microflow cytometer with oxygen control to diagnose and monitor sickle cell disease (SCD). This non-invasive method enables the analysis of individual cells under controlled oxygen conditions. The electrical impedance of healthy RBCs and sickle cells from three patients was measured in both normal (normoxic) and low (hypoxic) oxygen environments at frequencies of 156 kHz, 500 kHz, and 3 MHz. The results showed that healthy and sickle cells could be distinguished by their impedance at 156 kHz and 500 kHz under normoxic conditions, but not at 3 MHz. Significant impedance differences were observed in sickle cells both between patients and within individual patients' cells when comparing normoxic and hypoxic conditions across all frequencies. These findings suggest that electrical impedance can reflect disease status and detect sickling events in SCD. In a later study [88] (Fig. 4F), this system was further developed into a portable device. The portable device demonstrated sufficient sensitivity to differentiate between RBCs from healthy donors and those from SCD patients, making it a promising point-of-care tool for SCD diagnosis and monitoring.

Cell survival rate (CSR) is a vital metric in both biology and medicine. In a study by Zi et al. [89] (Fig. 4G), a microfluidic hypertonic stimulus-based impedance flow cytometry chip (HSIFC) was introduced to assess CSR. This approach utilizes a hypertonic stimulus to induce volume changes between live and dead cells, which are then distinguished through impedance measurements. The technique provides real-time CSR evaluation by leveraging the osmotic volume response of living cells. Similarly, Huang et al. [90] (Fig. 4H) presented a system for dynamic particle sizing and real-time measurement of individual cell membrane permeability. The device performs multiple cell impedance measurements (at up to ten time points) after exposure to different media, such as dimethyl sulfoxide (DMSO) or deionized water, introduced through separate inlets. Ten pairs of gold electrodes along a 20 mm microchannel enable these measurements, capturing data within 0.26 seconds post-mixing at a throughput of 150 samples per second. This allows precise tracking of cell volume changes due to osmosis in anisosmotic environments over 1.3 seconds, enabling accurate assessment of cell water permeability, as demonstrated for yeast cells.

4.4 Section summary

Monitoring cell responses to certain stimuli is critical to understanding cell properties (e.g., mechanical loading to assess deformability), as well as to optimize cell treatment protocols (e.g., electroporation for intracellular delivery). Compared to techniques that require labeling or fixation, MIC reduces the risk of altering cell behavior and allows for more natural observations. Moreover, multiple MIC sensing zones can be integrated into microfluidic systems thus allowing cell measurement before and after the stimulation, or even at different time points post stimulation. Furthermore, MIC data

collection and processing require limited memory and processing resources due to the 1D nature of impedance signals (compared e.g. to images), which also favors repeated or continuous measurements. Using MIC to monitor dynamic cell processes is among the promising future directions of the technique.

5 Integrating MIC with sample carrying/confinement

MIC has been used in combination with two main types of sample carrying/confinement systems: droplets (Section 5.1) and microcarriers (Section 5.2). An overview is reported in Table 4.

5.1 Droplet-based systems

Droplet-based microfluidic systems are versatile platforms that encapsulate materials within discrete droplets suspended in a carrier fluid. These systems minimize sample volume while enabling high throughput [91] and their applications span fields such as drug delivery, cellular studies, material synthesis, and chemical reaction monitoring [92]. The demand for automation, precision, and efficient analytical output has further driven the development of advanced detection techniques tailored to droplet-based analysis.

MIC represents an easy tool to characterize droplet size and velocity [92], and therefore can be used to optimize droplet production, even with online analysis and control. Besides that, MIC can be used to address the more challenging task of characterizing droplet content (e.g., cell in droplets). Panwar et al. [93] (Fig. 5A) demonstrated the MIC-based detection and counting of cells trapped in microdroplets. Specifically, water-in-oil droplets (~150 pL) were produced using a T-junction flow channel. The continuous phase consisted of fluorinated oil, while the dispersed phase contained RBCs suspended in Phosphate-Buffered Saline (PBS). The MIC signal featured a primary peak from the droplet and secondary peaks representing individual cells, allowing the counting of multiple cells within a single droplet. Zhong et al. [94] (Fig. 5B) presented a novel and highly precise method for monitoring bacterial growth by combining droplet microfluidics with electrochemical amplification. This system, called self-synchronized droplet-amplified electrical screening cytometry (SYNC), encapsulates individual bacterial cells within picoliter-sized droplets, enabling real-time, label-free detection of bacterial activity by measuring electrical impedance. Compared to conventional techniques, SYNC increases sensitivity fivefold and reduces detection time by 50%. Additionally, it allows for reliable detection at bacterial concentrations as low as 10^4 bacteria/ml. A droplet-based microfluidic impedance flow cytometer for in situ detection of microplastics in water was also recently reported [95]. Further works [96–98] that use droplets and impedance cytometry within microfluidic sorting systems are discussed in Section 6.

5.2 Microcarrier-based systems

Cell microcarriers are spherical 3D matrix scaffolds (100–400 µm in diameter) designed to enhance the scalability of cell cultures for tissue engineering and cell therapies.[99] These cultures can span several days to months, making real-time, label-free, and non-invasive monitoring of microcarrier conditions crucial for many bioprocesses. To meet this need, MIC has emerged as a promising approach.

Gong et al. [99] (Fig. 5C) demonstrated the continuous monitoring of individual hydrogel/Cytodex microcarriers using electrical impedance spectroscopy with co-planar Field's metal electrodes. Their method was validated through in vitro experiments where they monitored impedance changes during the growth of human skin keratinocytes (HaCaT) in GelMA hydrogel microcarriers and the differentiation of adipose-derived mesenchymal stem cells (ADSCs) on Cytodex 3 microcarriers. Their closed-loop system efficiently tracked both cell-encapsulated hydrogel and cell-attached Cytodex microcarriers via multi-dimensional impedance signals, distinguishing between adipogenic and osteogenic differentiation based on impedance profiles. This platform holds the potential for integration into bioreactors for long-term, remote monitoring of biomass and cell quality during bioprocessing.

In a recent study by Brandi et al. [100] (Fig. 5D) MIC was used to analyse innovative single-cell microcarriers called nanovials. These crescent-shaped microcarriers support cell adhesion, growth, and secretion while shielding cells from shear stress. The combination of nanovials with MIC presents a novel opportunity for high-throughput electrical analysis of single adherent cells. Brandi et al. utilized a simple cytometer with three coplanar electrodes to distinguish between free cells, empty nanovials, cell-loaded nanovials, and clusters, based on the electrical diameter at 0.5 MHz. Furthermore, the study investigated MIC's potential to assess the electrical phenotype of cells within nanovials showing potential for label-free viability assessments. MIC also shows promise for enhancing nanovial production and cell-loading protocols, offering a rapid and efficient characterization method. As a perspective, MIC analysis can be incorporated into cell analysis workflows that utilize nanovial technology, serving as an additional characterization step.

5.3 Section summary

The ability of electric current to penetrate through interfaces makes MIC an attractive choice to study cell in microcarriers or in confined systems compared to optical approaches, which may struggle in these conditions due to limited light penetration. Due to the non-invasiveness of MIC, its synergistic combination with microcarriers in closed-loop recirculating systems also enables repeated measurements over time for continuous online monitoring of cultures (e.g. bacterial proliferation, stem-cell differentiation), with direct applications in biomass remote monitoring. The number of applications featuring MIC analysis of cells in droplets or microcarriers is expected to increase in the future, also thanks to research

efforts aimed at developing MIC-tailored formulations with optimal conductivity.

6 Integrating MIC with a sorting functionality

One of the main attractiveness of MIC is its label-free nature, which favours low cost and simple sample preparation. Furthermore, the lack of labelling enables sample reuse after the analysis, even for cell therapy applications. Accordingly, adding a sorting functionality to a microfluidic impedance cytometer would greatly enhance its usefulness in applications. Several approaches for microfluidic single-cell sorting have been proposed in the literature (cf. e.g. refs. [101,102]). To develop an impedance-activated sorting system, MIC sensing must be coupled with an actuation mechanism, to displace selected particles towards designated outlets. Moreover, real-time processing of the MIC signals must be implemented, to instruct the actuator based on the current cell/particle properties. In the following, relevant examples of impedance-activated sorting systems are presented, grouped based on their actuation mechanism: DEP (Section 6.1), acoustic (Section 6.2), piezoelectric (Section 6.3), or valve-based (Section 6.4). An overview of these systems is reported in Table 5.

6.1 DEP sorting

One of the first demonstrations of impedance-activated sorting was presented by De Wageenar et al. [103] (Fig. 6A). They developed a microfluidic system aimed at selective sperm-cell refinement based on: (i) a DEP pre-focusing region, to control cell location and velocity; (ii) a MIC sensing region, to detect individual cells and identify the presence of cytoplasmic droplets on sperm flagella; (iii) a DEP sorting region, to deflect target particles based on impedance features. The acquisition and processing of the MIC signals as well as the active control of the DEP excitation were performed by a custom-built LabVIEW program. A proof-of-concept experiment of sorting beads and sperm cells was reported.

The combination of MIC sensing and DEP actuation was recently used by Lefevre et al. [104] to achieve selective and reconfigurable particle trajectory control (Fig. 6B). Specifically, they reported three operation modes on a mixture of beads (8, 10, and 12 µm diameter): (i) particle position swapping across the channel axis, irrespective of particle size, (ii) size-based particle separation, irrespective of particle position, and (iii) sorting of a selected sequence of particles. To implement the desired control logics, an innovative real-time signal processing algorithm was developed, written in C-language and running on a RISC processor embedded in the impedance spectroscope.

An original system developed by Panwar et al. [98] (Fig. 6C) integrates MIC sensing with fluorescence-activated DEP sorting to automate high-throughput droplet screening experiments. Specifically, impedance analysis is used to monitor the droplet frequency, spacing, and trajectory at the sorting junction in real time. This information is employed to continuously and automatically optimize all parameters and address any disturbances, resulting in higher throughput, better reproducibility, and enhanced robustness. The method uses field programmable gate array (FPGA)-powered high-speed computation for real-time processing and the control software (iSort) is available at Zenodo Database.

6.2 Acoustic sorting

Acoustic sorting offers a biocompatible, label-free approach to cell sorting, utilizing focused traveling surface acoustic waves (FTSAW) generated by a focused interdigitated transducer (FIDT) [105]. Ai's group [96,97,105,106] recently developed a microfluidic system capable of acoustic single-cell sorting, activated by MIC characterization. Real-time processing of impedance signals was achieved through an embedded system, programmed with a custom algorithm tailored for the specifically application.

In ref. [106] (Fig. 6D), the microfluidic system was employed to separate live MCF-7 cells from a mixed sample containing both live and fixed MCF-7 cells. The sorting throughput was over 100 cells per second with a purity rate of approximately 91.8%. A finite state machine (FSM) algorithm was developed to identify target cells based on transit time and impedance magnitude, and accordingly activate the acoustic sorting mechanism. In ref. [105], the microfluidic system was employed to assess and enrich viable cryopreserved human peripheral blood mononuclear cells (PBMCs) with a processing rate of up to 1000 cells per second. To accurately determine the viability of individual PBMCs based on their electrically measured complex opacity, a regional classification (RC) algorithm was developed to distinguish between live and dead cell populations.

Applications of the platform to droplet-based systems were also reported. The DUPLETS (Deformability-assisted dUal-Particle Encapsulation via Electrically acTivated Sorting) system [96], employs the platform to improve co-encapsulation of bead carriers and biological cells. The system evaluates droplet contents based on electrical impedance and transit time, distinguishing hydrogel beads from cell cytoplasm by deformability. DUPLETS improves both purity and throughput by discarding droplets with multiple cells or beads, overcoming limitations of existing co-encapsulation techniques. A similar system called SELECTS [97] (SElectable Label-free Encapsulated Cell-in-dropleT Sorting), uses an algorithm that determines cell quantity in droplets to enhance single-cell encapsulation. SELECTS achieves a 98.9% detection accuracy, rejecting around 90% of empty droplets and 60% with multiple cells, leading to a purity rate of 90.3% and a high throughput of up to 200 droplets per second. These systems [96,97], allowing controlled co-encapsulation of beads/cells, are crucial for applications like cancer immunotherapy and advanced biological assays.

6.3 Piezoelectric sorting

Piezoelectric actuators offer great opportunities for precise and low-cost control of fluids at the microscale [107]. A microfluidic cell sorter with integrated piezoelectric actuator offers notable features[108], such as low voltage operation (~10 Vpp) and low power consumption (0.1 mW), precise control of the magnitude of transverse cell deflection, and rapid response time (0.1–1 ms).

Gong et al. [109] developed a microfluidic platform that integrates a serpentine channel for particle focusing, two MIC sensing regions for particle characterization, and a piezoelectric actuator for particle sorting. An in-house multi-processing Python program is used for real-time impedance signal processing and sorting activation. The intended application is the label-free continuous inline monitoring and sorting for cell-based manufacturing. They demonstrated the accomplishment of four impedance-based sorting tasks: (i) sorting of microcarriers with high cell densities, (ii) sorting of microcarriers with osteogenic differentiated ADSCs, (iii) sorting of cell-encapsulated alginate microparticles of high cell viability, and (iv) sorting of 3D ADSC aggregates of specific sizes. A similar platform integrating sheath flow focusing, two MIC sensing regions, and a piezoelectric sorter was presented by Zhu et al. [110] (Fig. 6E). An FPGA is used for processing and control. The platform is designed to implement sample preparation before mass-spectrometry (MS), which has emerged as a significant label-free technique for the characterization of single-cell-level metabolomics and proteomics[111]. Simultaneously with sorting, target cells are transferred from the local high-salinity buffer to a MS-compatible solution (i.e., desalting), so that the collected cells can be directly fed for MS analysis. As a perspective, by coupling MIC and MS, a multimodal (i.e., electrical and metabolic) characterization of single cells may be achieved.

In contrast with refs. [109,110], dual membrane pumps[112] consisting of two piezoelectric actuators instead of one were used recently by Kui et al. [113] to achieve higher sorting efficiency. Using FPGA-based high-precision sort-timing prediction, the system accomplished low-latency (less than 0.3 ms), label-free, high-throughput (1000 particles per s) and high-accuracy (almost 99%) single-particle impedance-activated sorting.

The combination of MIC-sensing and piezoelectric actuation was also used in bioprinting applications. Schoendube et al. [114] (Fig. 6F) introduced a method that uses impedance-based cell detection to initiate drop-on-demand printing, allowing for the controlled delivery of single cells, in contrast to traditional random seeding. To this aim, a real-time algorithm running within the impedance spectroscope was used. Printing efficiency was 73% ± 11% for single polystyrene beads, and reasonable cell viability was maintained when printing cells (HeLa and fibroblasts).

6.4 Valve-based sorting

Elastomeric microvalves have found applications in various microfluidic fields, including flow cytometry. An elastomeric microvalve features a polydimethylsiloxane (PDMS) membrane that is actuated pneumatically and positioned between two channels. This design offers a response time in the milliseconds range, eliminates leakage and dead volume, and is relatively easy to manufacture [115].

Zhu et al. [116] (Fig. 6G) introduced a novel *Caenorhabditis elegans* (*C. elegans*) microfluidic impedance cytometry system (*Ce*MIC) that identifies worm developmental stages based on impedance signals and enables size-based enrichment by incorporating PDMS pneumatic valves and distributary channels downstream of the worm channel. A solenoid valve controlled by a microcontroller unit (MCU) is utilized to operate the pneumatic valves, while a custom MATLAB GUI program is used for real-time processing of the impedance signals and therefore worm-size identification. The effective separation of large and small worms is demonstrated. Choi et al. [117]presented a system for deformability-activated sorting of single particles. The deformability is measured by evaluating the transit time through a constriction based on electric current time traces. The latter are processed in real-time by a Labview program, and a threshold-based triggering signal is used to sort soft and rigid hydrogel beads by means of two high-speed solenoid valves.

6.5 Section summary

In recent years, various sorting mechanisms have been successfully integrated with MIC, including DEP, acoustic, piezoelectric, and valve-based sorting systems. This successful track-record is largely influenced by the simplicity and flexibility of the generic MIC setup, which can be integrated within most microfluidic systems. Acoustic and piezoelectric actuation generally allow for higher throughput, as high-voltage DEP-sorting combined with droplet encapsulation. As opposed to existing active cell separation techniques requiring markers which can possibly change the cellular properties or damage cells (e.g. fluorescence or magnetic activated cell sorting), MIC label-free analysis enables to sort cells not only as an endpoint but also as a pre-processing step in cell culture and biologics manufacturing. Additionally, the multiparametric information provided by MIC allows the sorting system to operate on multiple cell phenotypes, including electrical and mechanical properties. Aside from testing the technology on new biological targets (e.g. cryopreserved cells, cell aggregates, microcarriers), current research efforts are mostly focused on improving the sorting throughput (currently reaching 1,000 cells/second) and on the development of reconfigurable or multi-way sorting capabilities. As a perspective, translating current lab prototypes into a robust and easy-to-use commercial MIC-based sorter would significantly accelerate the adoption of the technology.

7 Discussion and perspective

The enduring vision of the lab-on-a-chip community is to realize highly integrated, miniaturized devices capable of performing complex laboratory functions on a single chip. The present review shows that the integration of MIC with other microfluidic tools enables the creation of systems for accurate multiparametric characterization of single-cells or cell-carrier complexes, possibly including on-chip sample preparation or stimulation steps, as well as sorting of selected subpopulations. Integrating all these functionalities (preparation, sensing, stimulation, sorting) in a single device, preferably with an automated control and the possibility to repeat each function at multiple times/locations, would open exciting perspectives for next generation single-cell analysis platforms, with applications ranging from life-science research to diagnostics, from bioprocess development to environmental monitoring.

On the other hand, many challenges must be undertaken to fulfil this vision, also considering the necessity to move from research prototypes to robust, affordable, and easy-to-use devices. Most of these challenges are not specific to MIC and apply to microfluidic lab-on-a-chip systems in general. For a discussion about relevant technological and commercial aspects see e.g. refs. [118–123]. Focusing on systems integrating MIC with other microfluidic tools, several key points can be identified that fall into three main categories: device structure, experimental setup, and signal-processing and control.

Device structure. Electrical impedance-based systems are conveniently configurable and can easily be automated and multiplexed[18]. They have a compact nature and high level of integration, making them suitable even to a wearable implementation[124]. Integrating MIC systems with other microfluidic tools requires that the potential impact on device complexity, portability and cost be carefully balanced with performance gains, depending on the specific application. Particularly interesting are all-electrical platforms, since they allow enhanced capabilities with minimal increase in system complexity. Examples already explored in the literature include platforms combining MIC-sensing and DEP-actuation, MIC-sensing and electroporation, or MIC-sensing and tools (such as microchannel profiles/structures) that do not require additional active fields and do not significantly increase the complexity of fluidic handling and control. As a long-term perspective, all-electrical cell service-stations integrating multiple MIC-sensing, DEP-actuation, electroporation, and electrical lysis (with even MIC-sensing of the lysed content) can be imagined.

Experimental setup. To achieve good MIC measurements, the cell suspension buffer must have suitable features. Specifically, its dielectric properties need to ensure high SNR and high contrast with cell dielectric properties over the probed frequency range. This requirement becomes more demanding when measuring cells in droplets or microcarriers, since the dielectric properties of the three components (buffer, cell, carrier) must be considered. Similarly, integrating MIC with other tools like DEP or electrophoresis may add different requirements on buffer dielectric properties, to ensure proper functioning avoiding electrode degradation or excessive Joule heating. Furthermore, certain types of on-chip sample stimulation may require tailored buffer modifications (e.g., increased viscosity for effective fluid-induced deformation) that need not impact the SNR negatively. Buffer osmolarity and density also require careful tuning, to avoid unwanted cell osmotic stress and mitigate particle sedimentation. Finally, some additional tools may require labelling steps, thus partly reducing the benefits of biophysical cytometry.

Another point of attention regards the flow rate, which affects particle velocity and throughput. In MIC, limitations on the flow rate derive from the sampling rate of the acquisition system (i.e., the event signals must be described by enough samples) and from the lowest stimulation frequency (which must be higher than the frequency content of the event signal). Other microfluidic tools may have different constraints. For instance, DEP-actuation may require lower flow rates to generate an effective particle displacement with reasonable voltages; inertial focusing or viscoelastic extensional flows may require higher flow rates to achieve effective focusing or cell deformation; additional sensing modalities (optical/image flow cytometry) may pose limitations arising from the characteristics of their hardware.

Optimization of the setup (e.g., buffer and carrier properties, electrode material, flow rates) through both numerical and experimental investigations is recommended. Strategies for on-chip buffer swap or flow rate modulation (e.g., ref. [63,125]) can also be considered.

Signal-processing and control. Integrating MIC with other microfluidic tools may require tailored signal processing. First, when combining MIC-sensing with other active tools (e.g., acoustic fields, microwaves, further electric fields) possible interferences may arise that must be removed (e.g., via filtering). For multimodal sensing approaches, the relevant data streams may have similar format (i.e., both time-domain signals, like MIC and microwave sensing) or different format (e.g., MIC and imaging), and a central question is how to combine the associated information. This can be done at the level of the raw data streams or at the feature level (i.e., after individual processing of the two raw data streams). In both cases, several solutions are possible depending on the specific application (e.g., regression or classification problems).

In case of impedance-activated sorting systems, MIC-signals must be processed in real-time to identify target versus non-target particles and to provide an estimate of particle velocity, which is needed for timely actuation. This calls for tailored algorithms and an associated hardware framework (microprocessors or FPGA for highest speed). Real-time monitoring of MIC-signals would also be useful during continuous monitoring from a bioreactor, since it would allow the implementation of a feedback loop to control process parameters.

On a broader perspective, increasing the functionalities of the microfluidic system to fulfil the lab-on-a-chip vision calls for a “brain” that controls the plumbing components and the actuation features by deciding tasks based upon the signals received from the sensing units. To accomplish this, AI-based solutions are highly promising, since they enable real-time perception and decision in complex tasks[126,127].

In summary, we believe that integrating MIC with other microfluidic tools offers tremendous opportunities to develop multifunctional intelligent platforms for single-cell analysis and we hope that interdisciplinary research efforts will overcome present challenges to realize this potential in the coming years.

Author Contributions

Conceptualization: F.C.; Methodology: F.C.; Investigation: C.B., M.R.; Data Curation: M.R., C.B., Writing - Original Draft: M.R., F.C.; Writing - Review & Editing: R.R., C.B.; Visualization: M.R., C.B., R.R., F.C.; Supervision: F.C.; Funding acquisition: F.C.

Conflicts of interest

There are no conflicts to declare.

Acknowledgements

This work was supported by the Italian Ministry of University and Research under the PRIN 2022 programme (MIC-AIM project, grant 2022245PTX), funded by European Union – Next Generation EU, Mission 4, Component 1 – CUP E53D23002530006.

References

1 K. C. M. Lee, J. Guck, K. Goda and K. K. Tsia, *Trends Biotechnol*, DOI:10.1016/j.tibtech.2021.03.006.

2 S.-S. Li, C.-D. Xue, Y.-J. Li, X.-M. Chen, Y. Zhao and K.-R. Qin, *Electrophoresis*, 2024, **45**, 1212–1232.

3 C. Honrado, P. Bisegna, N. S. Swami and F. Caselli, *Lab Chip*, 2021, **21**, 22–54.

4 S. Joo, K. H. Kim, H. C. Kim and T. D. Chung, *Biosens Bioelectron*, 2010, **25**, 1509–1515.

5 J. Zhong, D. Yang, Y. Zhou, M. Liang and Y. Ai, *Analyst*, 2021, **146**, 1848–1858.

6 A. De Ninno, R. Reale, A. Giovinazzo, F. R. Bertani, L. Businaro, P. Bisegna, C. Matteucci and F. Caselli, *Biosens Bioelectron*, 2020, **150**, 111887.

7 C. Honrado, A. Salahi, S. J. Adair, J. H. Moore, T. W. Bauer and N. S. Swami, *Lab Chip*, 2022.

8 C. Petchakup, P. E. Hutchinson, H. M. Tay, S. Y. Leong, K. H. H. Li and H. W. Hou, *Sens Actuators B Chem*, DOI:10.1016/j.snb.2021.129864.

9 S. A. Kruit, D. S. de Bruijn, M. L. W. J. Broekhuijse, W. Olthuis and L. I. Segerink, *Biosensors (Basel)*, 2022, **12**, 679.

10 C. Troiano, A. De Ninno, B. Casciaro, F. Riccitelli, Y. Park, L. Businaro, R. Massoud, M. L. Mangoni, P. Bisegna, L. Stella and F. Caselli, *ACS Sens*, 2023, **8**, 2572–2582.

11 D. C. Spencer, T. F. Paton, K. T. Mulroney, T. J. J. Inglis, J. M. Sutton and H. Morgan, *Nat Commun*, 2020, **11**, 5328.

12 T. Tang, X. Liu, Y. Yuan, R. Kiya, T. Zhang, Y. Yang, S. Suetsugu, Y. Yamazaki, N. Ota, K. Yamamoto, H. Kamikubo, Y. Tanaka, M. Li, Y. Hosokawa and Y. Yalikun, *Sens Actuators B Chem*, 2023, **374**, 132698.

13 J. S. McGrath, C. Honrado, J. H. Moore, S. J. Adair, W. B. Varhue, A. Salahi, V. Farmehini, B. J. Goudreau, S. Nagdas, E. M. Blais, T. W. Bauer and N. S. Swami, *Anal Chim Acta*, 2019, **1101**, 90–98.

14 T. Sun and H. Morgan, *Microfluid. Nanofluid.*, 2010, **8**, 423–443.

15 C. Petchakup, K. H. H. Li and H. W. Hou, *Micromachines (Basel)*, 2017, **8**, 87.

16 H. Daguerre, M. Solsona, J. Cottet, M. Gauthier, P. Renaud and A. Bolopion, *Lab Chip*, 2020, **20**, 3665–3689.

17 S. Zhu, X. Zhang, Z. Zhou, Y. Han, N. Xiang and Z. Ni, 2021, preprint, DOI: 10.1016/j.talanta.2021.122571.

18 F. Gökçe, P. S. Ravaynia, M. M. Modena and A. Hierlemann, *Biomicrofluidics*, DOI:10.1063/5.0073457.

19 T. Tang, T. Julian, D. Ma, Y. Yang, M. Li, Y. Hosokawa and Y. Yalikun, 2023, preprint, DOI: 10.1016/j.aca.2023.341424.

20 A. De Ninno, V. Errico, F. R. Bertani, L. Businaro, P. Bisegna and F. Caselli, *Lab Chip*, 2017, **17**, 1158–1166.

21 T. Tang, X. Liu, R. Kiya, Y. Shen, Y. Yuan, T. Zhang, K. Suzuki, Y. Tanaka, M. Li, Y. Hosokawa and Y. Yalikun, *Biosens Bioelectron*, DOI:10.1016/j.bios.2021.113521.

22 M. Shaker, L. Colella, F. Caselli, P. Bisegna and P. Renaud, *Lab Chip*, 2014, **14**, 2548–2555.

23 D. Holmes, D. Pettigrew, C. H. Reccius, J. D. Gwyer, C. Van Berkel, J. Holloway, D. E. Davies and H. Morgan, *Lab Chip*, 2009, **9**, 2881–2889.

24 D. Barat, D. Spencer, G. Benazzi, M. C. Mowlem and H. Morgan, *Lab Chip*, 2012, **12**, 118–126.

25 N. Haandbæk, O. With, S. C. Bürgel, F. Heer and A. Hierlemann, *Lab Chip*, 2014, **14**, 3313–3324.

26 N. Haandbæk, S. C. Bürgel, F. Rudolf, F. Heer and A. Hierlemann, *ACS Sens*, 2016, **1**, 1020–1027.

27 Y. Feng, L. Huang, P. Zhao, F. Liang and W. Wang, *Anal Chem*, 2019, **91**, 15204–15212.

28 X. Zou, D. C. Spencer, J. Chen and H. Morgan, *RSC Adv.*, 2024, **14**, 34270–34278.

29 D. Holmes, J. K. She, P. L. Roach and H. Morgan, *Lab Chip*, 2007, **7**, 1048–1056.

30 D. Spencer, G. Elliott and H. Morgan, *Lab Chip*, 2014, **14**, 3064–3073.

31 P. Simon, M. Frankowski, N. Bock and J. Neukammer, *Lab Chip*, 2016, **16**, 2326–2338.

32 C. Honrado, L. Ciuffreda, D. Spencer, L. Ranford-Cartwright and H. Morgan, *J R Soc Interface*, DOI:10.1098/rsif.2018.0416.

33 H. Liang, Y. Zhang, D. Chen, Y. Li, Y. Wang, J. Wang and J. Chen, *Journal of Micromechanics and Microengineering*, DOI:10.1088/1361-6439/ac5171.

34 P. Rees, H. D. Summers, A. Filby, A. E. Carpenter and M. Doan, *Nature Reviews Methods Primers*, 2022, **2**, 86.

35 M. Daorazio, R. Reale, A. De Ninno, M. A. Brighetti, A. Mencattini, L. Businaro, E. Martinelli, P. Bisegna, A. Travaglini and F. Caselli, *IEEE Trans Biomed Eng*, 2022, **69**, 921–931.

36 M. Kokabi, M. Tayyab, G. M. Rather, A. Pournadali Khamseh, D. Cheng, E. P. DeMauro and M. Javanmard, *Biomed Microdevices*, DOI:10.1007/s10544-024-00707-0.

37 X. Chen, H. Liang, Y. Li, D. Chen, J. Wang and J. Chen, *IEEE Trans Electron Devices*, 2022, **69**, 6408–6416.

38 X. Huang, X. Chen, H. Tan, M. Wang, Y. Li, Y. Wei, J. Zhang, D. Chen, J. Wang, Y. Li and J. Chen, *Cytometry Part A*, 2024, **105**, 139–145.

39 S. Chen, X. Chen, X. Huang, Z. Fang, J. Wang, X. Huo, X. Chen and J. Chen, *IEEE Nanotechnol Mag*, DOI:10.1109/MNANO.2024.3513132.

40 U. Tefek, B. Sari, H. Z. Alhmoud and M. S. Hanay, *Advanced Materials*, DOI:10.1002/adma.202304072.

41 Y. C. Alatas, U. Tefek, B. Kucukoglu, N. Bardakci, S. Salehin and M. S. Hanay, *IEEE Sens J*, 2024, **24**, 16085–16092.

42 S. Yan and D. Yuan, 2021, preprint, DOI: 10.1016/j.talanta.2020.121401.

43 T. Peng, J. Qiang and S. Yuan, 2023, preprint, DOI: 10.3389/fbioe.2023.1331968.

44 X. Xuan, J. Zhu and C. Church, 2010, preprint, DOI: 10.1007/s10404-010-0602-7.

45 U. D. Larsen, G. Blankenstein and J. Branebjerg, in *International Conference on Solid-State Sensors and Actuators, Proceedings*, 1997, vol. 2.

46 C. Bernabini, D. Holmes and H. Morgan, *Lab Chip*, 2011, **11**, 407–412.

47 H. Choi, C. S. Jeon, I. Hwang, J. Ko, S. Lee, J. Choo, J. H. Boo, H. C. Kim and T. D. Chung, *Lab Chip*, DOI:10.1039/c4lc00238e.

48 M. Evander, A. J. Ricco, J. Morser, G. T. A. Kovacs, L. L. K. Leung and L. Giovangrandi, *Lab Chip*, 2013, **13**, 722–729.

49 R. Scott, P. Sethu and C. K. Harnett, *Review of Scientific Instruments*, DOI:10.1063/1.2900010.

50 R. Rodriguez-Trujillo, O. Castillo-Fernandez, M. Garrido, M. Arundell, A. Valencia and G. Gomila, *Biosens Bioelectron*, DOI:10.1016/j.bios.2008.04.005.

51 M. Wang, J. Zhang, X. Chen, Y. Li, X. Huang, J. Wang, Y. Li, X. Huo and J. Chen, *Microsyst Nanoeng*, 2024, **10**, 192.

52 J. H. Nieuwenhuis, F. Kohl, J. Bastemeijer, P. M. Sarro and M. J. Vellekoop, *Sens Actuators B Chem*, DOI:10.1016/j.snb.2003.10.017.

53 J. Zhu, Y. Feng, H. Chai, F. Liang, Z. Cheng and W. Wang, *Lab Chip*, DOI:10.1039/d3lc00178d.

54 D. Spencer and H. Morgan, *Lab Chip*, 2011, **11**, 1234–1239.

55 Y. Zhou, J. Wang, T. Liu, M. Wu, Y. Lan, C. Jia and J. Zhao, *Analyst*, DOI:10.1039/d3an00726j.

56 W. Tang, D. Tang, Z. Ni, N. Xiang and H. Yi, *Anal Chem*, 2017, **89**, 3154–3161.

57 D. Tang, M. Chen, Y. Han, N. Xiang and Z. Ni, *Sens Actuators B Chem*, 2021, **336**, 129719.

58 C. Grenvall, C. Antfolk, C. Z. Bisgaard and T. Laurell, *Lab Chip*, 2014, **14**, 4629–4637.

59 X. Xie, Z. Zhang, X. Ge, X. Zhao, L. Hao, Z. Cheng, W. Zhou, Y. Du, L. Wang, F. Tian, F. Tian and X. Xu, *Anal Chem*, 2019, **91**, 13398–13406.

60 M. A. Mansor, M. A. Jamrus, C. K. Lok, M. R. Ahmad, M. Petrů and S. S. R. Koloor, *Sensors and Actuators Reports*, 2025, **9**, 100277.

61 S. I. Han and K. H. Han, *Anal Chem*, 2015, **87**, 10585–10592.

62 C. Raillon, J. Che, S. Thill, M. Duchamp, B. X. E. Desbiolles, A. Millet, E. Sollier and P. Renaud, *Cytometry Part A*, 2019, **95**, 1085–1095.

63 C. Petchakup, H. M. Tay, K. H. H. Li and H. W. Hou, *Lab Chip*, 2019, **19**, 1736–1746.

64 C. Petchakup, Y. Y. C. Chen, H. M. Tay, H. B. Ong, P. Y. Hon, P. P. De, T. W. Yeo, K. H. H. Li, S. Vasoo and H. W. Hou, *ACS Sens*, 2023, **8**, 3136–3145.

65 X. Han, C. Van Berkel, J. Gwyer, L. Capretto and H. Morgan, *Anal Chem*, 2012, **84**, 1070–1075.

66 N. N. Watkins, U. Hassan, G. Damhorst, H. K. Ni, A. Vaid, W. Rodriguez and R. Bashir, *Sci Transl Med*, DOI:10.1126/scitranslmed.3006870.

67 U. Hassan, N. N. Watkins, B. Reddy, G. Damhorst and R. Bashir, *Nat Protoc*, 2016, **11**, 714–726.

68 K. Torres-Castro, J. Jarmoshti, L. Xiao, A. Rane, A. Salahi, L. Jin, X. Li, F. Caselli, C. Honrado and N. S. Swami, *Adv Mater Technol*, DOI:10.1002/admt.202201463.

69 C. H. Lee, H. Seok, W. Jang, J. T. Kim, G. Park, H. U. Kim, J. Rho, T. Kim and T. D. Chung, *Biosens Bioelectron*, DOI:10.1016/j.bios.2021.113499.

70 Y. Zhou, D. Yang, Y. Zhou, B. L. Khoo, J. Han and Y. Ai, *Anal Chem*, 2018, **90**, 912–919.

71 R. Reale, A. De Ninno, T. Nepi, P. Bisegna and F. Caselli, *IEEE Trans Biomed Eng*, 2023, **70**, 565–572.

72 E. M. Darling and D. Di Carlo, *Annual Reviews Inc.*, 2015, preprint, DOI: 10.1146/annurev-bioeng-071114-040545.

73 J. Kim, H. Lee and S. Shin, *J Cell Biotechnol*, 2015, **1**, 63–79.

74 Y. Chen, K. Guo, L. Jiang, S. Zhu, Z. Ni and N. Xiang, 2022, preprint, DOI: 10.1016/j.talanta.2022.123815.

75 D. Yang, Y. Zhou, Y. Zhou, J. Han and Y. Ai, *Biosens Bioelectron*, 2019, **133**, 16–23.

76 P. Ghassemi, X. Ren, B. M. Foster, B. A. Kerr and M. Agah, *Biosens Bioelectron*, DOI:10.1016/j.bios.2019.111868.

77 Z. Han, L. Chen, S. Zhang, J. Wang and X. Duan, *Anal Chem*, 2020, **92**, 14568–14575.

78 Y. Feng, H. Chai, W. He, F. Liang, Z. Cheng and W. Wang, *Small Methods*, DOI:10.1002/smtd.202200325.

79 Y. Feng, J. Zhu, H. Chai, W. He, L. Huang and W. Wang, *Small*, DOI:10.1002/smll.202303416.

80 J. Jarmoshti, A.-B. Siddique, A. Rane, S. Mirhosseini, S. J. Adair, T. W. Bauer, F. Caselli and N. S. Swami, *Small*, **n/a**, 2407212.

81 C. Petchakup, H. Yang, L. Gong, L. He, H. M. Tay, R. Dalan, A. J. Chung, K. H. H. Li and H. W. Hou, *Small*, 2022, **18**, 2104822.

82 L. He, J. Tan, S. Y. Ng, K. H. H. Li, J. Han, S. Y. Chew and H. W. Hou, *Adv Mater Technol*, DOI:10.1002/admt.202400589.

83 J. Chen, X. Zou, D. C. Spencer and H. Morgan, *Microsyst Nanoeng*, 2024, **10**, 173.

84 M. Zheng, J. J. Sherba, J. W. Shan, H. Lin, D. I. Shreiber and J. D. Zahn, *Technology (Singap World Sci)*, 2017, **05**, 31–41.

85 S. C. Bürgel, C. Escobedo, N. Haandbæk and A. Hierlemann, *Sens Actuators B Chem*, 2015, **210**, 82–90.

86 Y. Ye, X. Luan, L. Zhang, W. Zhao, J. Cheng, M. Li, Y. Zhao and C. Huang, *Micromachines (Basel)*, DOI:10.3390/MI11090856.

87 J. Liu, Y. Qiang, O. Alvarez and E. Du, *Sens Actuators B Chem*, 2018, **255**, 2392–2398.

88 D. Dieujuste, Y. Qiang and E. Du, *Biotechnol Bioeng*, 2021, **118**, 4041–4051.

89 Q. Zi, W. Ding, C. Sun, S. Li, D. Gao, L. He, J. Liu, L. Xu and B. Qiu, *Biosens Bioelectron*, DOI:10.1016/j.bios.2019.111820.

90 L. Huang, J. D. Benson and M. Almasri, *Anal Chim Acta*, DOI:10.1016/j.aca.2021.338441.

91 A. Kalantarifard, A. Saateh and C. Elbuken, *MDPI Multidisciplinary Digital Publishing Institute*, 2018, preprint, DOI: 10.3390/chemosensors6020023.

92 A. Saateh, A. Kalantarifard, O. T. Celik, M. Asghari, M. Serhatlioglu and C. Elbuken, *Lab Chip*, 2019, **19**, 3815–3824.

93 J. Panwar and R. Roy, *Microelectron Eng*, DOI:10.1016/j.mee.2019.111010.

94 J. Zhong, Y. Chang, M. Liang, Y. Zhou and Y. Ai, *Biosens Bioelectron*, DOI:10.1016/j.bios.2024.116397.

95 M. Aghel, S. Fardindoost, N. Tasnim and M. Hoorfar, *Environments*, DOI:10.3390/environments11050096.

96 J. Zhong, M. Liang and Y. Ai, *Small Methods*, DOI:10.1002/smtd.202300089.

97 J. Zhong, M. Liang, Q. Tang and Y. Ai, *Mater Today Bio*, DOI:10.1016/j.mtbio.2023.100594.

98 J. Panwar, R. Utharala, L. Fennelly, D. Frenzel and C. A. Merten, *Cell Reports Methods*, 2023, **3**, 100478.

99 L. Gong, C. Petchakup, P. Shi, P. L. Tan, L. P. Tan, C. Y. Tay and H. W. Hou, *Small*, DOI:10.1002/smll.202007500.

100 C. Brandi, A. De Ninno, F. Ruggiero, E. Limiti, F. Abbruzzese, M. Trombetta, A. Rainer, P. Bisegna and F. Caselli, *Lab Chip*, 2024, **24**, 2883–2892.

101 Y. Shen, Y. Yalikun and Y. Tanaka, *Sens Actuators B Chem*, 2019, **282**, 268–281.

102 N. Lu, H. M. Tay, C. Petchakup, L. He, L. Gong, K. K. Maw, S. Y. Leong, W. W. Lok, H. B. Ong, R. Guo, K. H. H. Li and H. W. Hou, *Lab Chip*, 2023, **23**, 1226–1257.

103 B. de Wagenaar, S. Dekker, H. L. de Boer, J. G. Bomer, W. Olthuis, A. Van Den Berg and L. I. Segerink, *Lab Chip*, 2016, **16**, 1514–1522.

104 A. Lefevre, C. Brandi, A. De Ninno, F. Ruggiero, E. Verona, M. Gauthier, P. Bisegna, A. Bolopion and F. Caselli, *Lab Chip*, 2024.

105 J. Zhong, P. Li, M. Liang and Y. Ai, *Adv Mater Technol*, DOI:10.1002/admt.202100906.

106 P. Li and Y. Ai, *Anal Chem*, 2021, **93**, 4108–4117.

107 C. Brandi, A. De Ninno, E. Verona, L. Businaro, P. Bisegna and F. Caselli, *Sens Actuators A Phys*, DOI:10.1016/j.sna.2024.115074.

108 C. H. Chen, S. H. Cho, F. Tsai, A. Erten and Y. H. Lo, *Biomed Microdevices*, DOI:10.1007/s10544-009-9341-5.

109 L. Gong, L. He, N. Lu, C. Petchakup, K. H. H. Li, C. Y. Tay and H. W. Hou, *Adv Healthc Mater*, **n/a**, 2304529.

110 J. Zhu, S. Pan, H. Chai, P. Zhao, Y. Feng, Z. Cheng, S. Zhang and W. Wang, *Small*, **n/a**, 2310700.

111 T. Xu, D. Feng, H. Li, X. Hu, T. Wang, C. Hu, X. Shi and G. Xu, *TrAC Trends in Analytical Chemistry*, 2022, **157**, 116763.

112 S. Sakuma, Y. Kasai, T. Hayakawa and F. Arai, *Lab Chip*, DOI:10.1039/c7lc00536a.

113 K. Zhang, Z. Xia, Y. Wang, L. Zheng, B. Li and J. Chu, *Lab Chip*, 2024, **24**, 4918–4929.

114 J. Schoendube, D. Wright, R. Zengerle and P. Koltay, *Biomicrofluidics*, 2015, **9**, 14117.

115 B. Y. Yu, C. Elbuken, C. Shen, J. P. Huissoon and C. L. Ren, *Sci Rep*, DOI:10.1038/s41598-018-21833-9.

116 Z. Zhu, W. Chen, B. Tian, Y. Luo, J. Lan, D. Wu, D. Chen, Z. Wang and D. Pan, *Sens Actuators B Chem*, 2018, **275**, 470–482.

117 G. Choi, R. Nouri, L. Zarzar and W. Guan, *Microsyst Nanoeng*, DOI:10.1038/s41378-019-0107-9.

118 U. A. Gurkan, D. K. Wood, D. Carranza, L. H. Herbertson, S. L. Diamond, E. Du, S. Guha, J. Di Paola, P. C. Hines, I. Papautsky, S. S. Shevkoplyas, N. J. Sniadecki, V. K. Pamula, P. Sundd, A. Rizwan, P. Qasba and W. A. Lam, 2024, preprint, DOI: 10.1039/d3lc00796k.

119 S. Battat, D. A. Weitz and G. M. Whitesides, *Lab Chip*, DOI:10.1039/d1lc00731a.

120 M. I. Mohammed, S. Haswell and I. Gibson, *Procedia Technology*, DOI:10.1016/j.protcy.2015.07.010.

121 Y. Temiz, R. D. Lovchik, G. V. Kaigala and E. Delamarche, 2015, preprint, DOI: 10.1016/j.mee.2014.10.013.

122 D. R. Reyes, H. Van Heeren, S. Guha, L. Herbertson, A. P. Tzannis, J. Ducree, H. Bissig and H. Becker, 2021, preprint, DOI: 10.1039/d0lc00963f.

123 S. Dekker, P. K. Isgor, T. Feijten, L. I. Segerink and M. Odijk, *Microsyst Nanoeng*, 2018, **4**, 34.

124 A. Furniturewalla, M. Chan, J. Sui, K. Ahuja and M. Javanmard, *Microsyst Nanoeng*, 2018, **4**, 20.

125 X. Huang, K. Torres-Castro, W. Varhue, A. Rane, A. Rasin and N. S. Swami, *Electrophoresis*, DOI:10.1002/elps.202100304.

126 D. McIntyre, A. Lashkaripour, P. Fordyce and D. Densmore, *Lab Chip*, 2022, **22**, 2925–2937.

127 J. Zheng, T. Cole, Y. Zhang, J. Kim and S.-Y. Tang, *Biosens Bioelectron*, 2021, **194**, 113666.

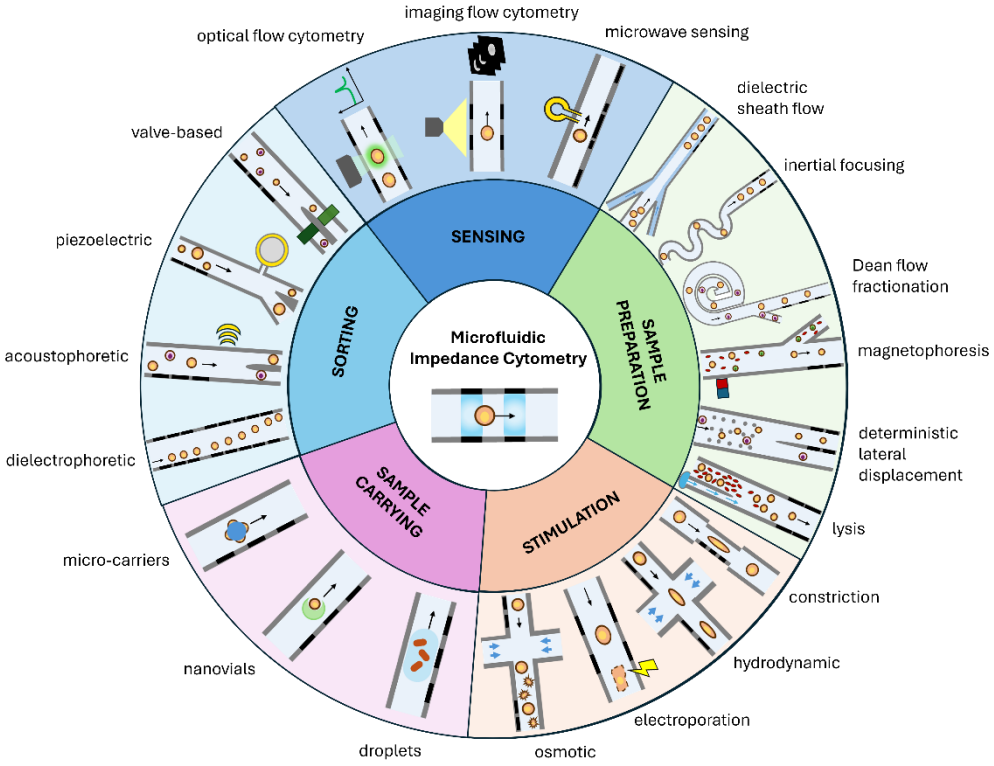

Fig. 1 Diagram showing combinations of microfluidic impedance cytometry with other microfluidic tools. Five categories are identified, according to their synergistic advantage: improving the multiparametric characterization capability by including an additional sensing modality, enabling on-chip sample preparation steps before the impedance measurement, stimulating the sample to elicit behaviours of interest, sample carrying/confinement to provide tailored support or microenvironment, and impedance-activated sample sorting.

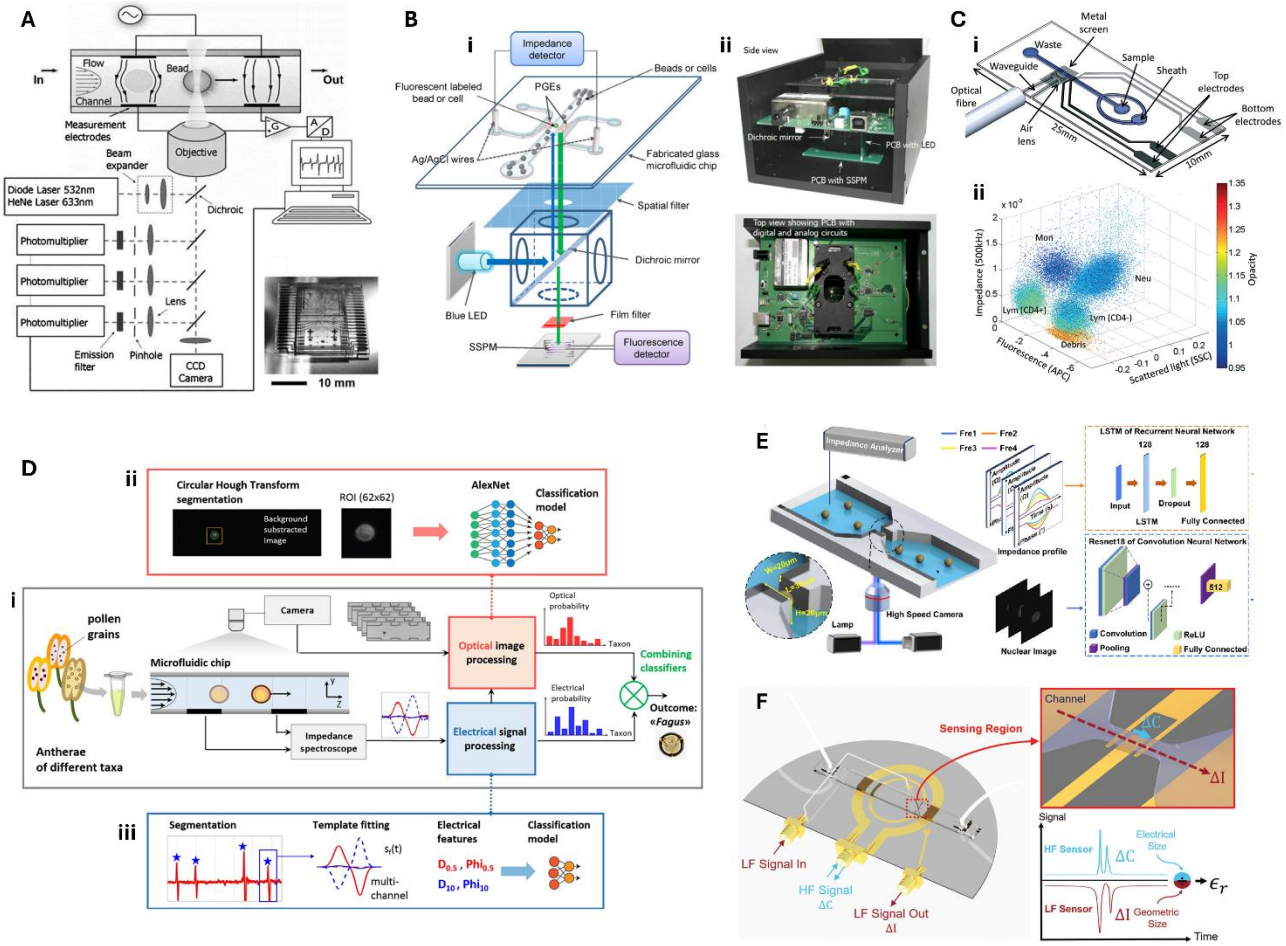

Fig. 2. Examples of microfluidic systems integrating MIC-sensing with and additional sensing modality. (A) Schematic diagram of the system developed in ref. [29], showing the optical and electrical detection setup and photograph of an individual micro-chip. (B) System developed in ref. [4]: i) schematic diagram showing simultaneous detection of impedance and fluorescence; ii) pictures of the device (side view and top view). (C) i) Schematic diagram of the system from ref. [30], showing the electrodes, the integrated waveguide, and the optical fibre for light delivery; ii) 3D scatter plot for WBCs for side scatter, fluorescence and low-frequency impedance (data point coloured according to electrical opacity). (D) i) Multimodal analysis approach to pollen classification proposed in ref. [35], along with the processing workflows for ii) electrical signals and (iii) optical images. (E) Schematic of the imaging and impedance flow cytometer by ref. [38]. (F) Microfluidic platform by ref. [40] integrating two electronic sensors: a low-frequency (LF) sensor and a high-frequency (HF) microwave sensor. Images were adapted with permission from (A) ref. [29], copyright The Royal Society of Chemistry 2007, (B) ref. [4], copyright 2009 Elsevier B.V., (C) ref. [30], copyright The Royal Society of Chemistry 2014, (D) ref. [35], copyright 2021 IEEE, (E) ref. [38], copyright 2023 International Society for Advancement of Cytometry, (F) ref. [40], copyright 2023 The Author(s).

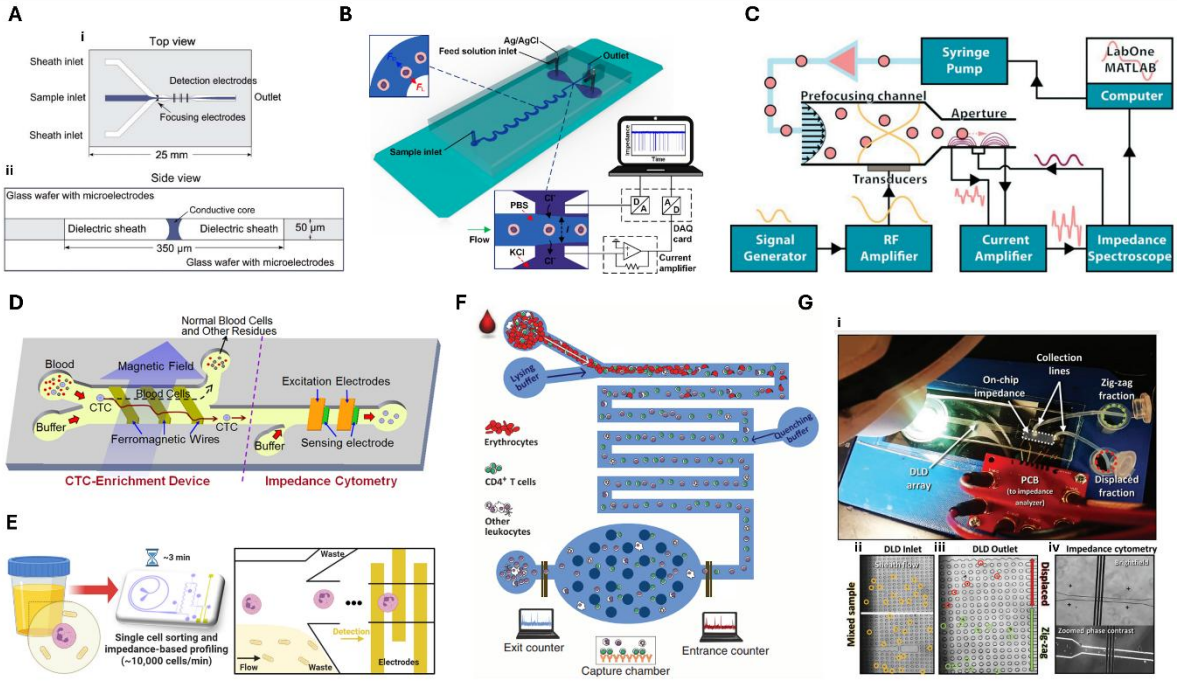

Fig. 3: Examples of microfluidic systems integrating MIC-sensing with on-chip sample preparation. (A) i) Top view and ii) side view schematics of the dielectric focusing approach developed in ref. [48] (B) Working principle of the system by ref. [56]: an asymmetric serpentine structure and elasto-inertial focusing yield consistent cross-sectional position of tumor cells prior to MIC measurement. (C) Schematic of the experimental setup by ref. [58]: a computer-controlled syringe pump sends the suspension into the chip where particles/cells are acoustophoretically prefocused using a 2D acoustic standing wave field prior to MIC sensing. (D) Perspective view of the system described in ref. [61], composed of the CTC-enrichment device, based on lateral magnetophoresis, followed by MIC sensing. (E) Illustration of rapid screening of urinary tract infection using the integrated impedance cytometer developed in ref. [64]. (F) Graphical schematic of the microfluidic system presented in ref. [66], enabling on-chip erythrocyte lysis from blood and differential T-cell count before and after a capture chamber (for CD4+ or CD8+ T-cells). (G) Integrated device developed in ref. [68] : i) top view of PCB connections to the impedance electrodes, as well as collection of DLD separated fractions; ii) images of mixed sample flowing into the inlet; iii) separated fraction at the end of the DLD array; iv) on-chip impedance measurement of displaced cells. Images were adapted with permission from: (A) ref. [48], copyright The Royal Society of Chemistry 2013, (B) ref. [56], copyright 2017 American Chemical Society, (C) ref. [58], copyright The Royal Society of Chemistry 2014, (D) ref. [61], copyright 2015 American Chemical Society, (E) ref. [64], copyright 2023 American Chemical Society, (F) ref. [66], copyright 2013 by the American Association for the Advancement of Science, (G) ref. [68], copyright 2023 The Author(s).

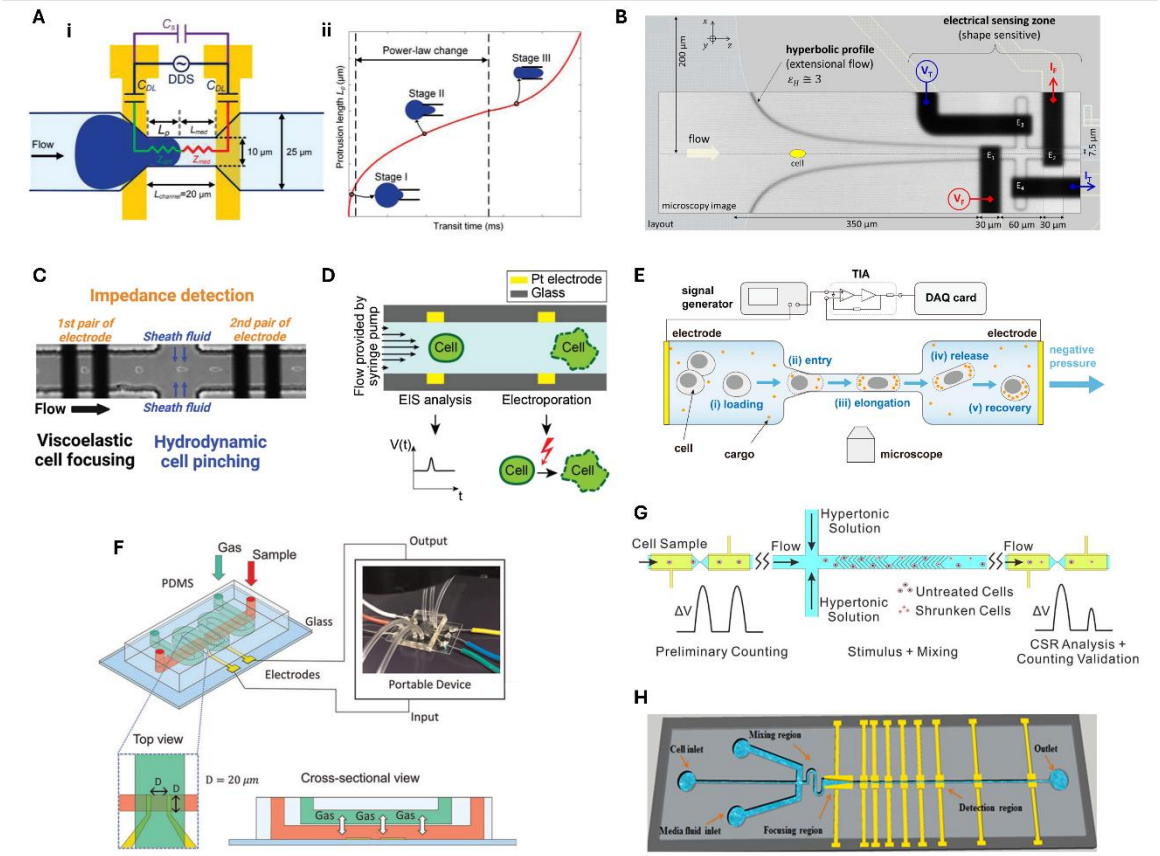

Fig. 4 Examples of microfluidic systems integrating MIC-sensing with on-chip sample stimulation. (A) Single-cell intrinsic mechanical characterization by ref. [78]: i) equivalent impedance-deformability mapping model and ii) protrusion length time-course. (B) Layout of the system developed in ref. [71] consisting of a hyperbolic microchannel, inducing cell deformation by extensional flow, equipped with shape-sensitive MIC electrodes. (C) Brightfield image illustrating hydrodynamic cell deformation by sheath fluid at the channel cross junction, by ref. [81]. (D) Cross-sectional schematic of the chip from ref. [85]: a pair of electrodes for electroporation upon passage of a cell, and a separate set of two facing electrodes for EIS measurements. (E) Schematic of the microfluidic system for single-cell electroporation and impedance assessment from ref. [86] (TIA, trans-impedance amplifier, DAQ, data acquisition). (F) Schematics and picture of the portable MIC system with oxygen control developed in ref. [88]. (G) Design principle of the microfluidic hypertonic stimulus-based impedance flow cytometry chip from ref. [89]. (H) Schematic of the microfluidic platform structure for membrane permeability measurement by ref. [90]. Images were adapted with permission from (A) ref. [78], copyright 2022 Wiley-VCH GmbH, (B) ref. [71], copyright 2022 IEEE, (C) ref. [81], copyright 2022 Wiley-VCH GmbH, (D) ref. [85], copyright 2014 Elsevier B.V., (E) ref. [86], copyright 2020 The Authors, (F) ref. [88], copyright 2021 Wiley Periodicals LLC, (G) ref. [89], copyright 2019 Elsevier B.V., (H) ref. [90], copyright 2021 Elsevier B.V.

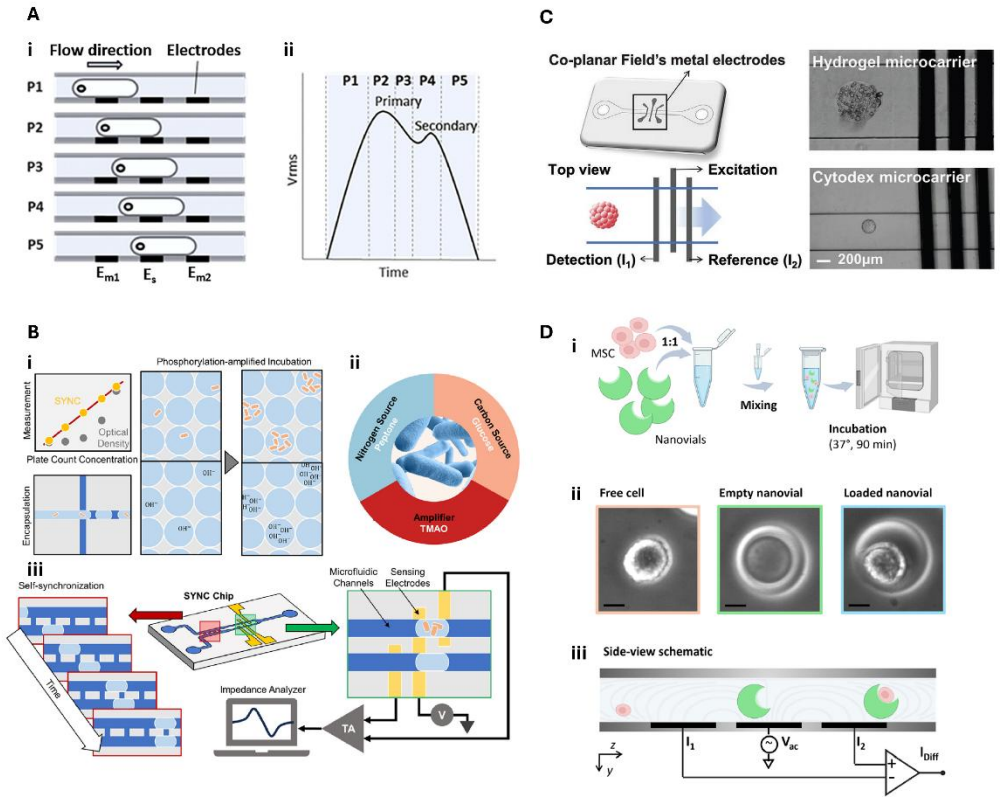

Fig. 5 Examples of systems for MIC analysis of cells carried in droplets/microcarriers. A) Concept proposed in ref. [93]: i) droplet containing a single cell at specific positions relative to the microelectrode array (Em1, Em2: measuring electrodes, Es: source electrode), along with ii) plot of the contribution of each position to differential signal (only positive peak is displayed). (B) i) Schematic of the SYNC system proposed in ref. [94], involving droplet emulsion and electrochemical modifications; ii) the composition of a specially engineered bacterial culture medium; iii) the SYNC chip design featuring self-synchronization and electrical detection regions. (C) Schematic illustration of device from ref. [99] along with brightfield images of hydrogel microcarrier (top) and Cytodex 3 microcarrier (bottom). (D) Combining MIC with nanovial technology as proposed in ref. [100]: i) sample preparation (MSC, mesenchymal stromal cells); ii) microscopy images of a free cell, an empty nanovial, and a cell loaded nanovial (10 µm scale bar); iii) schematic of the MIC sensing zone. Images were adapted with permission from (A) ref. [93], copyright 2019 Elsevier B.V., (B) ref. [94], copyright 2024 Elsevier B.V., (C) ref. [99], copyright 2021 Wiley-VCH GmbH, (D) ref. [100], copyright The Royal Society of Chemistry 2024.

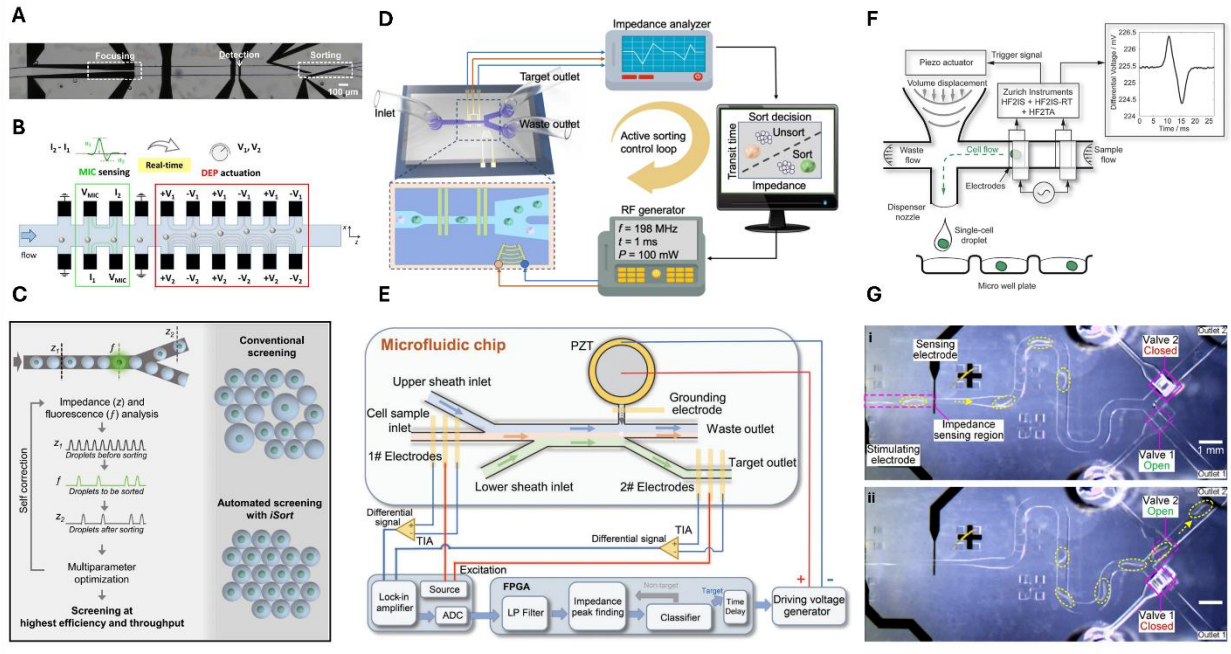

Fig. 6: Examples of impedance-based sorting systems. (A) Microfluidic chip for DEP-focusing, MIC-detection, and DEP-sorting of sperm cells, developed in ref. [103]. (B) Schematic representation of the platform for MIC-sensing and DEP-based trajectory control introduced in ref. [104]. (C) Illustration of high-throughput automated droplet screening, by ref. [98]. (D) Schematic setup of the impedance-activated sorting system presented in ref. [106] (E) Schematic setup of the one-step sorting and desalting system proposed in ref. [110]. (F) Working principle of on-demand impedance-activated cell printing from ref. [114]. (G) Enrichment of large *C. elegans* worms with the system described in ref. [116]: time-stacked images showing the dynamic process of steering a large worm for sample collection, i) before and ii) after the valve switching. Images were adapted with permission from (A) ref. [103], copyright The Royal Society of Chemistry 2016, (B) ref. [104], copyright The Royal Society of Chemistry 2024, (C) ref. [98], copyright 2023 The Authors, (D) ref. [106], copyright American Chemical Society, (E) ref. [110], copyright 2024 Wiley-VCH GmbH, (F) ref. [114], copyright 2015 AIP Publishing LLC, (G) ref. [116], copyright 2018 Elsevier B.V.

Table 1 Microfluidic systems integrating MIC-sensing with an additional sensing modality (ASM, additional sensing modality; CM, Clausius-Mossotti; CNN, convolutional neural network; CV, coefficient of variation; DC, direct current; FACS, fluorescence activated cell sorting; GFP, green fluorescent protein; LED, light emitting diode; LOD, limit of detection; MIC, microfluidic impedance cytometry; MMT, Maxwell's mixture theory; PGE, polyelectrolyte gel electrodes; PMT, photomultiplier tube; RNN, recurrent neural network; SSPM, solid-state photomultiplier; YAG, yttrium-aluminium-garnet)

ASM type	ASM description	MIC description	ASM role	MIC role	Performance metrics	Aim of the work	Ref.
Optical flow cytometry	Dual laser (solid state YAG + HeNe) for excitation; bandpass filters and PMTs for collection	2 pairs of facing electrodes; 100 kHz-10 MHz frequency range	Measurement of antibody binding by fluorescence at 3 wavelengths ranges (585 nm, 675 nm, and >715 nm)	To determine particle size and to trigger fluorescence signal capture	LOD: ~2.6×10^4 fluorescent molecules per bead; 1 µm size resolution (in 2 µm-10 µm size range)	Bead-based immunoassays using a micro-chip flow cytometer	[29] (Fig. 2A)
	LED (460-475 nm) for excitation; film filter and SSPM for collection	1 pair of facing PGE electrodes; DC	Detection and classification of fluorescent cells/particles	To provide information on the number and size distribution of microparticles and cells	Calculated GFP transfection ratio (*i.e.*, number of fluorescence peaks over the number of impedance peaks) very close to that measured by a FACS machine (99% and 98%, respectively)	A portable microfluidic flow cytometer based on simultaneous detection of impedance and fluorescence	[4] (Fig. 2B)
	Diode laser (635 nm) coupled to an integrated waveguide for excitation; filter set and PMTs for collection	2 pairs of facing electrodes; 0.5 MHz and 2 MHz frequency	Measurement of fluorescence and large-angle side scattering to distinguish between CD4+ and CD4− lymphocytes	Electrical characterization (low frequency impedance and opacity)	Excellent size accuracy (CVs ≤ 2.1%), sensitivity and dynamic range (3.5 orders of magnitude) at sample flow rates of 80 µL per minute	A sheath-less combined optical and impedance micro-cytometer	[30] (Fig. 2C)
	Sapphire laser 488 nm for excitation; multi-mode optical fibre and PMT for collection	2 pairs of facing electrodes; 300 kHz-10 MHz frequency range	Measurement of side scattering and fluorescence (validation only) for monocyte/granulocyte classification	Electrical characterization (impedance magnitude, ratio of reactance at 10 MHz to resistance at 2.3 MHz)	LOD for particle volumes: ~2 fL (i.e., 1.5 µm diameter)	Label-free whole blood cell differentiation based on multifrequency MIC and light scatter analysis	[31]
	Laser (488 nm) for excitation; microscope objective, dichroic mirror, filters, and PMT for detection	2 pairs of facing electrodes; reference frequency at 18.3 MHz, probe frequency in the 250 kHz-50 MHz range	Fluorescence detection (525 nm) used to unambiguously identify parasites by their GFP expression within the host cell	Electrical characterization (dielectric properties based on multi-shell model and MMT)	Parasitaemias calculated by fluorescence-coupled MIC close to those determined by microscopy; goodness of MMT fits: average $R^2 > 0.997$	Dielectric characterization of *P. falciparum*-infected red blood cells	[32]
	Metal halide lamp and bandpass filter for excitation; Zinc oxide layer for masking; PMT tube plus a bandpass filter for fluorescence detection	2 electrodes in secondary microchannels; 40 kHz and 100 kHz frequency	Structural characterization (nuclear diameter estimated from fluorescence pulse profile)	Electrical characterization (cell diameter, cytoplasmic conductivity and specific membrane capacitance estimated from impedance amplitude and phase profiles)	Success rate of cell-type classification ranging from 79.5% to 90.9% (in five 2-class problems involving different cell types)	Characterization of single-cell intrinsic structural and electrical parameters	[33]
Imaging flow cytometry	High-speed camera mounted on a bright-field microscope	2 pairs of coplanar electrodes in lateral chambers; 0.5 MHz and 10 MHz frequency	To determine class probability based on deep feature extraction from images	To determine class probability based on electrical diameters and phases; identification of cell-containing frames	84.2% balanced accuracy and 88.3% accuracy, in an 8-class pollen classification task	Classification of pollen grains with a multimodal electro-optical approach	[35](Fig. 2D)
	High-speed camera mounted on a bright-field microscope	2 coplanar electrodes; 8 frequencies: 100 kHz, 250 kHz, 500 kHz, 750 kHz, 1 MHz, 1.25 MHz, 1.5 MHz, and 1.75 MHz	Optical characterization (particle diameter)	Electrical characterization (signal peak at different frequencies)	94.9% average test accuracy, in a 4-class classification task	Integration of electrical and optical features through a multimodal approach for particle classification	[36]

	High-speed camera mounted on a fluorescence microscope	2 electrodes in secondary microchannels; 40 kHz and 100 kHz frequency	Structural characterization based on traditional or deep feature extraction from nuclear images	Electrical characterization based on traditional or deep feature extraction from impedance profiles	Success rates of 88.3% (traditional feature extraction) and 100% (deep feature extraction) in a 3-class cell classification problem	Cell classification using six key bio-structural and bioelectrical parameters	[37]
	High-speed camera mounted on a fluorescence microscope	Plug-in electrode wires; 60 kHz, 700 kHz, 990 kHz, and 2.5 MHz frequency	Structural characterization based on nuclear images processed by a CNN	Electrical characterization based on impedance profiles processed by an RNN	100% accuracy in a 2-class cell classification problem	High throughput characterization of single-cell electrical and structural properties	[38] (Fig. 2E)
Microwave sensing	Split ring microwave (≈5 GHz) resonator	2 coplanar electrodes; 500 kHz frequency	To yield capacitance, function of the geometrical size and the CM factor of the particle that depends on the particle's electrical permittivity	Determination of the geometrical size of the particle to normalize the microwave signal	94.9% accuracy in the binary classification of polystyrene and glass microparticles	Permittivity-based microparticle classification by the integration of MIC and microwave resonators	[40] (Fig. 2F)

Table 2 Microfluidic systems integrating MIC-sensing with on-chip sample selection/enrichment (CCAM, cyclone-cytometer integrated air monitor; CTC, circulating tumor cell; DC, direct current; DFF, Dean flow fractionation; LPS, lipopolysaccharide; MIC, microfluidic impedance cytometry; PBMC, peripheral blood mononuclear cells; UTI, urinary tract infection)

Principle	Task	Sample Composition	MIC description	Aim of the work	Ref.
Magnetophoresis: ferromagnetic permalloy wire array	Enrichment of CTCs	CTCs (labelled with immunomagnetic nanobeads and graphene nanoplates) spiked into whole blood	2 pairs of facing electrodes; 500 kHz and 10 MHz frequency	CTCs electrical characterization	[61] (Fig. 3D)
Inertial: Vortex technology	Purification of cancer cells	MCF7 human breast cancer cell line; human colon cancer cell lines (LoVo, HT-29); PBMCs; polystyrene beads	2 coplanar electrodes; 460 kHz or 500 kHz and 2 MHz frequency	Isolation, enumeration and sizing of CTCs	[62]
Inertial: DFF sorter and asymmetric serpentine focuser	Selection of neutrophils, in addition to improving MIC consistency	Neutrophils from lysed or diluted blood; PBMCs from whole blood; samples were spiked with beads	3 coplanar electrodes; 0.3 MHz and 1.7 MHz frequency	Report of a "sample-in-answer-out" integrated platform for continuous leukocyte sorting and single-cell electrical profiling (neutrophil functional characterization toward diabetes testing)	[63]
Inertial: DFF sorter and asymmetric serpentine focuser	Selection of neutrophils, in addition to improving MIC consistency	Neutrophils from blood samples of non-UTI donors; neutrophils incubated with *E. coli* suspensions; urine samples from UTI patients and healthy donors; samples were spiked with beads	3 coplanar electrodes; 0.3 MHz, 1.72 MHz and 12 MHz frequency	Rapid UTI tests	[64] (Fig. 3E)
Lysis module	Selective lysis of red blood cells	Whole blood from healthy donors and patients (full range of pathological samples)	2 pairs of facing electrodes; 444 kHz and 1.776 MHz frequency	Counting and electrical characterization of lymphocytes, monocytes, granulocytes	[65]
Lysis module and immunocapture chamber	Selective lysis of red blood cells and selective capturing of $CD4^+$ and $CD8^+$ T-cells	Whole blood	2 sets of 3 coplanar electrodes; 303 kHz and 1.7 MHz frequency	Enumeration of $CD4^+$ and $CD8^+$ T-cells in 30 min using 10 µl of blood	[66] (Fig. 3F) and [67]
Deterministic Lateral Displacement	Size-based separation of activated vs non-activated macrophages	Macrophages Raw 264.7 cells (untreated or LPS treated); polystyrene beads	3 coplanar electrodes; 0.5 MHz, 2 MHz, 18 MHz frequency	To develop a hybrid platform for monitoring the separation of specific subpopulations from cellular samples with wide size distributions (application toward enrichment of activated macrophages)	[68] (Fig. 3G)
Wet-cyclone air sampler	Sucking the air and concentrating the bioaerosols into 10 mL of aqueous solvent	Aerosolized suspension of *E. coli* or beads	2 Ag/AgCl electrodes; DC	To build a CCAM for differentiation of aerosolized microbeads, dust, and *E. coli*	[69]

Table 3 Microfluidic systems integrating MIC-sensing with on-chip sample stimulation (CAF, cancer associated fibroblasts; CSR, cell survival rate; CTC, circulating tumor cell; iPSCs, induced pluripotent stem cells; MIC, microfluidic impedance cytometry; n.i., not indicated; PDAC, pancreatic ductal adenocarcinoma; SCPCs, spinal cord progenitor cells)

Type	Principle	MIC analysis	MIC description	Aim of the work	Ref.
Mechanical stimulation	Microconstriction channel	Passage time, entry time, transit time, impedance magnitude	4 sets of 2 coplanar electrodes; 1 MHz frequency	Simultaneous mechanical and electrical characterization of individual biological cells in a high-throughput manner	[70]
	Differential microcostriction channel with 4 successive constrictions\relaxation regions	Total transit time (deformability), individual transit times, average impedance, relaxation index	4 self-aligned 3D electrodes; 50 kHz frequency	High-throughput biophysical phenotyping (deformability, electrical impedance, and relaxation index) of single cells	[75]
	Microcostriction channel	Profiles of impedance magnitude and phase as cells transit through the constriction channel	2 coplanar electrodes; 8 simultaneous frequencies in the 500 Hz-1 MHz range	Post-enrichment enumeration and characterization of CTCs	[76]
	Microconstriction channel	Impedance opacity and passage time	2 sets of 2 coplanar electrodes; 500 kHz and 5 MHz frequency	Simultaneous mechanical and electrical characterization of single plant cells	[77]
	Microconstriction channel	Measured resistance is proportional to the protrusion length, which depends on cell mechanical properties through a tailored model	2 coplanar electrodes (sensing zone); 1 MHz frequency	Camera-free intrinsic mechanical cytometry for on-the-fly measurement of single-cell Young's modulus and fluidity	[78] (Fig. 4A)
	Microconstriction channel	Analysis of the impedance profiles at multiple frequencies, coupled with electrical and mechanical models	3 coplanar electrodes; 4 frequencies: 250 kHz, 450 kHz, 750 kHz, and 1.2 MHz frequency	Multimodal electrical-mechanical single-cell characterization (Young's modulus, fluidity, radius, cytoplasm conductivity, and specific membrane capacitance)	[79]
	Hydrodynamic: hyperbolic channel profile to induce cell deformation by viscoelastic extensional flow	Electrical diameters measured along two orthogonal directions and their ratio (anisotropy index)	4 coplanar electrodes in cross configuration; 500 kHz and 615 kHz frequency	Contactless and optics-free erythrocyte deformability analysis	[71] (Fig. 4B)
	Hydrodynamic: hyperbolic channel profile to induce cell deformation by viscoelastic extensional flow plus a recovery zone	Peak, peak-to-peak, and width features extracted from the complex impedance profiles and their combinations	3 sets of 3 coplanar electrodes (pre-deformation, deformation, recovery); 0.5 MHz and 18 MHz frequency	Deformability analysis of heterogeneous cell populations with wide size distribution, and application to PDAC cells and CAFs	[80]
	Hydrodynamic: cell pinching at a cross junction by sheath fluids at a higher flow rate	Impedance magnitude at multiple frequencies and their ratios	2 sets of 2 coplanar electrodes (native and deformed); 0.3 MHz, 1.72 MHz, and 12 MHz frequency	Multiparametric biophysical analysis (cell size, cell deformability, membrane opacity, and nucleus opacity) and application to neutrophil mechanophenotyping and detection of low-abundance iPSCs from SCPCs	[81] (Fig. 4C) and [82]
	Hydrodynamic: viscoelastic shear flow	Impedances measured along two orthogonal directions and their ratio (electrical deformability)	5 pairs of facing electrodes; 0.5 MHz and 5 MHz frequency	Simultaneous electrical and optical deformability measurement, and application to untreated and treated (cytochalasin D, latrunculin B and glutaraldehyde) HL-60 cells	[83] and [28]
Electrical stimulation	Electroporation through an on-chip pair of facing microelectrodes (2 kV/cm, 50 kHz)	Impedance magnitude and phase at multiple frequencies, and fitting of impedance spectra (based on an equivalent circuit and the three-shell model)	1 pair of facing electrodes; 20 kHz-20 MHz frequency range	On-chip manipulation, electroporation, and impedance spectroscopy of single-cells, allowing to assess the same cell at multiple time points or to average the results of multiple passages of the same cell	[85] (Fig. 4D)
	Electroporation through 2 coplanar electrodes and a constriction; 5 pulse durations (0.2, 0.8, 1.0, 3.0, or 5.0 ms) and 5 electric fields (0.44, 0.58, 0.70, 0.87, or 1.05 kV/cm) tested	Resistive pulse-based detection, to trigger the administration of an electroporation pulse; current jumps as indicators of membrane permeabilization	2 coplanar electrodes (same used for electroporation); 1.224 kHz frequency	To develop a flow-based electroporation microdevice that automatically detects, electroporates, and monitors individual cells for changes in permeability and delivery	[84]
	Electroporation through a pair of Ag microelectrodes (0-3 V) and a constriction	Channel impedance variation in time	1 pair of Ag microelectrodes (same used for electroporation); 1 kHz frequency	Precise and rapid single-cell electroporation and simultaneous impedance monitoring in a constriction microchannel	[86] (Fig. 4E)
Physico-chemical stimulation	Oxygen control through a double-layer microfluidic channel to induce normoxic and hypoxic conditions (top layer: serpentine shape gas channel, bottom layer: thin gas-permeable membrane with a straight channel for cell suspension)	Impedance magnitude and phase at multiple frequencies	3 coplanar electrodes; 156 kHz, 500 kHz, and 3 MHz frequency (portable device: 2 coplanar electrodes; 100 kHz frequency)	A MIC device with oxygen control for measuring cellular response to hypoxia (with application to the detection of sickle cells), along with its portable implementation	[87] and [88] (Fig. 4F)
	Osmotic stimulation (exposure to hypertonic NaCl solution enhanced by on-chip mixing) to induce a	Impedance amplitude at low frequency (volume information)	2 sets of 2 coplanar electrodes (before and after	On-chip label-free determination of CSR	[89] (Fig. 4G)

volume difference between living and dead cells		exposure, to cross-verify counting); 450 kHz frequency		
Osmotic stimulation (exposure to anisosmotic extracellular media enhanced by on-chip mixing) to induce cell volume changes	Impedance variation across subsequent electrode pairs (after establishing the impedance-volume relationship)	10 pairs of coplanar electrodes; 100 Hz, 1 kHz, 10 kHz or 100 kHz frequency	Dynamic particle sizing and real-time individual cell membrane permeability measurement	[90] (Fig. 4H)

Table 4 Examples of systems for MIC analysis of cells carried in droplets/microcarriers (ADSC, adipose-derived mesenchymal stem cells; GelMA, gelatin methacryloyl; MIC, microfluidic impedance cytometry; PBS, phosphate buffered saline; SYNC, self-synchronized droplet-amplified electrical screening cytometry)

Carrier description	Sample description	MIC description	MIC analysis	Aim of the work	Ref.
Water-in-oil droplets generated in a T-junction microfluidic channel; average droplet volume ~150 pL	Droplet composition: human erythrocytes suspended in 1× PBS	3 coplanar 'in-contact' Field's metal electrodes; 1 MHz frequency	To detect and count the number of entrapped cells based on peak features in MIC signals	Cell-in-droplet quantification with a MIC-device using easy-to-fabricate electrodes	[93] (Fig. 5A)
Droplets in oil phase, 40 µm diameter	Droplet composition: *E. coli* and *K. pneumoniae* suspended in engineered culture medium	3 coplanar electrodes situated beneath a dual-channel detection region; 5 MHz frequency	To monitor bacterial growth based on impedance peaks and using auto-unbiasing for calibration	SYNC system for bacterial growth kinetic real-time monitoring	[94] (Fig. 5B)
Droplets in oil phase	Droplet composition: polystyrene microbeads (0.5 µm, 1 µm, 3 µm, or 6 µm diameter) dispersed in DI water at 0.05%, 0.10% or 0.20% solid particle percentage	3 coplanar electrodes; 4.4 MHz, 11 MHz, and 22.5 MHz frequency	Detection of microplastics based on impedance magnitude and phase	Development of a system for in situ detection of micropollutants in water	[95]
Hydrogel (GelMA) microcarriers and Cytodex 3 microcarriers beads; 100-400 µm diameter range	Human skin keratinocytes (encapsulated in hydrogel) and ADSCs (on Cytodex surface)	3 coplanar electrodes; 60 kHz and 1 MHz frequency	To monitor cell growth (hydrogel microcarriers) or cell differentiation (Cytodex microcarriers) based on impedance magnitudes and opacity	Direct and label-free monitoring of cell-microcarrier complexes using MIC, for biomanufacturing applications	[99] (Fig. 5C)
Single-cell crescent-shaped microcarriers (Biotinylated Nanovials, EZM™ formulation), 35 µm outer diameter	Human mesenchymal stromal cells loaded on Nanovial cavity by incubation	3 coplanar electrodes; 0.5 MHz frequency	Discrimination among free cells, empty nanovials, cell-loaded nanovials and clusters, based on the electrical diameter; potential for cell viability assay	Combination of nanovial technology with MIC for the electrical analysis of single adherent cells at high throughput	[100] (Fig. 5D)

Table 5 Examples of impedance-based sorting systems (ADSC, adipose-derived mesenchymal stem cells; DC, direct current; DEP, dielectrophoresis; DMSO, dimethyl sulfoxide; FIDT, focused interdigitated transducer; FPGA, field programmable gate array; FTSAW, focused travelling surface acoustic wave; GUI, graphical user interface; MCU, micro-controller unit; MIC, microfluidic impedance cytometry; PBMC, peripheral blood mononuclear cells; PDMS, polydimethylsiloxane; PEGDA, polyethylene glycol diacrylate; PS, polystyrene; RBC, red blood cells; RISC, reduced instruction set computer; RT, real-time)

Principle	Description	Sample composition	Sorting task(s) and throughput	RT processing	MIC description	Aim of the work	Ref.
DEP	2 pairs of top-down electrodes (15 MHz, 2 V)	Fresh boar semen, polystyrene beads	Sort beads from sperm cells; <5 cells/s	LabVIEW program running on a computer	2 (detection) or 1 (sorting) electrode pair; 1 MHz or 1.3 MHz frequency	Detection of cytoplasmic droplets in sperms and sorting of beads from sperm cells, towards microfluidic sperm refinement	[103] (Fig. 6A)
	6 pairs of coplanar electrodes in lateral chambers (400 kHz, 0-10.5 V)	Polystyrene beads of 3 sizes	Particle-position swapping, size-based particle separation, sorting of a desired particle sequence; 1 particles/s	RT algorithm written in C running on a RISC processor embedded in the impedance spectroscope	2 pairs of coplanar electrodes in lateral chambers; 3 MHz frequency	To develop an all-electrical platform for selective and reconfigurable single-particle manipulation	[104] (Fig. 6B)
	2 high-voltage 3D electrodes (DC, 0.5 kV- 1.6 kV)	Aqueous droplets encapsulating Mycl-9E10 hybridoma cells or beads	Reduce false positive events; up to 320 Hz	FPGA-powered high-speed computation	3 coplanar electrodes; 10 kHz frequency	To develop a method to automate droplet screening for phenotypic single-cell analysis, improving efficiency and stability	[98] (Fig. 6C)
Acoustic	FTSAW generated by FIDTs (198 MHz, 100 mW)	MCF-7 cells, PEGDA hydrogel beads, PS beads	Sorting of live MCF-7 cells from a mixture of fixed and live MCF-7; >100 cells/s	RT program running on a microprocessor embedded in the impedance analyzer	2 sets of 2 coplanar electrodes; 1 MHz frequency	Analyze and sort cells based on multivariate (electrical and mechanical) biophysical phenotyping	[106] (Fig. 6D)
	FTSAW generated by FIDTs (195 MHz, 300 mW)	Thawed primary PBMCs with different treatments (natural apoptosis, DMSO toxicity treatment, and freeze-shock)	Sorting of viable cells from dead cells and debris; up to 1000 cells/s	RT program running on a microprocessor embedded in the impedance analyzer	3 coplanar electrodes; 1-18 MHz frequency range	Integrated cell viability assay and on-demand enrichment of viable cells, with application to cryopreserved cells	[105]
	FTSAW generated by FIDTs (132 MHz, 6.3 mW)	Aqueous droplets with MCF-7 cells and PEGDA hydrogels	Sorting of single-paired cell-bead droplets; >60 droplets/s	RT program running on a microprocessor embedded in the impedance analyzer	2 sets of 2 coplanar electrodes; 500 kHz frequency	Improve co-encapsulation of bead carriers and biological cells via a combined mechanical and electrical screening	[96]
	FTSAW generated by FIDTs (132 MHz, 50 mW)	MCF-7 cells in droplets	Sorting of droplets with single cells or with multi-cells or empty droplets; up to 200 Hz	RT program running on a microprocessor embedded in the impedance analyzer	2 sets of 2 coplanar electrodes; 40 MHz frequency	Selectable cell quantity encapsulation in droplets sorting system	[97]
Piezoelectric	Piezoelectric actuator (75 Hz)	Cytodex-3 microcarrier, alginate microparticles, ADSC aggregates	Sorting of: microcarriers with high cell densities or osteogenic differentiated ADSCs, cell-encapsulated alginate microparticles, 3D ADSC aggregates; 5-10 particles/s	RT sensing and actuation using an in-house Python program running on a computer	2 coplanar electrodes; 60 kHz, 95 kHz, and 1.7 MHz frequency	To develop a platform for in-line sample processing from bioreactors and automated cell analysis, for quality control in continuous cell-based manufacturing	[109]
	Piezoelectric actuator driven with a high-voltage signal	PBMCs, HeLa cells, MDA-MB-468 cells, MCF-10A cells, RBCs, microbeads	Sorting of cancer cells (HeLa) from blood cells (PBMCs or RBCs) or sorting cancer (MDA-MB-468) form normal (MCF-10A) breast cells; >300 cells/s	FPGA-based signal processing and triggering	2 sets of 3 coplanar electrodes; 100 kHz and 15 MHz frequency	To develop a one-step sample preparation system (sorting and desalting) for efficient single-cell mass spectrometry	[110] (Fig. 6E)
	Dual membrane pumps consisting of two piezoelectric actuators	HeLa, MDA-MB-231, and Jurkat cells, polystyrene beads	Microbead size-based sorting, Jurkat and MDA-MB-231 cell sorting; Up to 1000 cells/s	FPGA-based signal processing and high-precision sort-timing prediction	3 coplanar electrodes; 0.5 MHz-50 MHz frequency range	High-throughput and high-accuracy single-cell sorting	[113]
	Piezo stack actuator deflecting a silicon membrane	PS beads, HeLa cells, human primary fibroblasts	Detect particle passage and timely trigger the piezo actuator to dispense the particle; 9 events/min	RT-algorithm running within the impedance spectroscope	2 pairs of facing electrodes; 500 kHz-10 MHz frequency range	Printing of single living cells encapsulated in droplets, as opposed to random seeding	[114] (Fig. 6F)
Valve-based	Solenoid valve connected to PDMS pneumatic valves (150 kPa compressed air)	*C. elegans* worms	Separation of large and small worms; 30 worms/min	Solenoid valve controlled via an MCU; impedance spectroscope and MCU controlled with a custom MATLAB GUI	1 pair of coplanar electrodes; 300 kHz frequency	Identification of worm developmental stage and size-based enrichment of worms	[116] (Fig. 6G)

	Two high-speed solenoid valves connected to a pressure source (typically 0.3 psi)	7.5% and 14% PEGDA hydrogel beads, to represent soft and rigid particles, respectively	Separation of soft and rigid beads; 600 particles/min	LabVIEW program	1 pair of Ag/AgCl electrodes; DC	To sort particles based on their deformability	[117]